Cellular/Molecular

Interaction via a Key Tryptophan in the I–II Linker of N-Type Calcium Channels Is Required for β1 But Not for Palmitoylated β2, Implicating an Additional Binding Site in the Regulation of Channel Voltage-Dependent Properties

Jérôme Leroy,[1] Mark S. Richards,[1,2]* Adrian J. Butcher,[1]* Manuela Nieto-Rostro,[1] Wendy S. Pratt,[1] Anthony Davies,[1] and Annette C. Dolphin[1]

[1]Laboratory of Cellular and Molecular Neuroscience, Department of Pharmacology, University College London, London WC1E 6BT, United Kingdom, and [2]School of Crystallography, Birkbeck College, London WC1E 7HX, United Kingdom

The $Ca_V\beta$ subunits of voltage-gated calcium channels regulate these channels in several ways. Here we investigate the role of these auxiliary subunits in the expression of functional N-type channels at the plasma membrane and in the modulation by G-protein-coupled receptors of this neuronal channel. To do so, we mutated tryptophan 391 to an alanine within the α-interacting domain (AID) in the I–II linker of $Ca_V2.2$. We showed that the mutation W391 virtually abolishes the binding of $Ca_V\beta1b$ and $Ca_V\beta2a$ to the $Ca_V2.2$ I–II linker and strongly reduced current density and cell surface expression of both $Ca_V2.2/\alpha2\delta\text{-}2/\beta1b$ and/$\beta2a$ channels. When associated with $Ca_V\beta1b$, the W391A mutation also prevented the $Ca_V\beta1b$-mediated hyperpolarization of $Ca_V2.2$ channel activation and steady-state inactivation. However, the mutated $Ca_V2.2W391A/\beta1b$ channels were still inhibited to a similar extent by activation of the D_2 dopamine receptor with the agonist quinpirole. Nevertheless, key hallmarks of G-protein modulation of N-type currents, such as slowed activation kinetics and prepulse facilitation, were not observed for the mutated channel. In contrast, $Ca_V\beta2a$ was still able to completely modulate the biophysical properties of $Ca_V2.2W391A$ channel and allow voltage-dependent G-protein modulation of $Ca_V2.2W391A$. Additional data suggest that the concentration of $Ca_V\beta2a$ in the proximity of the channel is enhanced independently of its binding to the AID by its palmitoylation. This is essentially sufficient for all of the functional effects of $Ca_V\beta2a$, which may occur via a second lower-affinity binding site, except trafficking the channel to the plasma membrane, which requires interaction with the AID region.

Key words: **calcium channel; neuron; α-interaction domain; β subunit; trafficking; G-protein; palmitoylation**

Introduction

Voltage-gated calcium (Ca_V) channels play a major role in the physiology of excitable cells, particularly of neurons. Three families of voltage-gated calcium channels have been identified, Ca_V1–Ca_V3 (for review, see Ertel et al., 2000). The Ca_V1 class, L-type channels and the Ca_V2 class, non-L-type channels are both high-voltage-activated (HVA). These are heteromultimers composed of the pore-forming α1 subunit, associated with auxiliary $Ca_V\beta$ and α2δ subunits (for review, see Catterall, 2000). The Ca_V2 calcium channels are inhibited by Gβγ dimers (Herlitze et al., 1996; Ikeda, 1996), which is the main mechanism of presynaptic inhibition by G-protein-coupled receptors. $Ca_V\beta$ subunits are crucial for normal HVA channel function (for review, see Dolphin, 2003a), because they enhance expression of functional channels at the plasma membrane, modulate their biophysical properties, and promote the voltage dependence of modulation of $Ca_V2.2$ calcium channels by Gβγ dimers, although the mechanism involved remains unclear (Bichet et al., 2000; Meir et al., 2000; Canti et al., 2001). Gβγ dimers and $Ca_V\beta$ subunits have been shown to bind to overlapping sites in the I–II loop of Ca_V2 channels, and they induce opposite effects on biophysical properties of the channels (for review, see Dolphin, 2003b), shifting channels between a willing and a reluctant state that requires large depolarizations to be opened (Bean, 1989). This observation led to the hypothesis that the binding of Gβγ dimers might dissociate the $Ca_V\beta$ subunit from the I–II loop of the α1 subunit (Sandoz et al., 2004) and that dissociation of $Ca_V\beta$ was the mechanism responsible for the inhibition observed. However, there is also evidence that Gβγ dimers do not displace $Ca_V\beta$ subunits but alter the orientation of the subunit with respect to the α1 subunit (Hummer et al., 2003).

Received March 23, 2005; revised June 13, 2005; accepted June 15, 2005.

This work was supported by The Wellcome Trust. We thank the following for generous gifts of cDNAs: Dr. Y. Mori (Seriken, Okazaki, Japan) for rabbit $Ca_V2.2$, Dr. M. Rees (University College London, London, UK) for mouse α2δ-2, Dr. E. Perez-Reyes (Loyola University, Chicago, IL) for rat β2a, Dr. P. G. Strange (Reading, UK) for rat D_2 dopamine receptor, M. Simon (California Institute of Technology, Pasadena, CA) for bovine Gβ1 and Gγ2, Dr. L. Birnbaumer for the β2a-β1b chimera, T. E. Hughes (Yale University, New Haven, CT) for mut-3 GFP, and Genetics Institute (Cambridge, MA) for pMT2. We thank Dr. P. Viard and Dr. K. Page for critical reading of this manuscript. We also thank K. Chaggar and L. Douglas for technical assistance.

*M.S.R. and A.J.B contributed equally to this work.

Correspondence should be addressed to Dr. Jérôme Leroy, Laboratory of Cellular and Molecular Neuroscience, Department of Pharmacology, University College London, Gower Street, London WC1E 6BT, UK. E-mail: j.leroy@ucl.ac.uk.

DOI:10.1523/JNEUROSCI.1137-05.2005

 0270-6474/05/256984-13$15.00/0

Here, we investigated the role of $Ca_V\beta$ subunits in the plasma membrane expression and G-protein modulation of $Ca_V2.2$ calcium channels by mutating the tryptophan (W391) in the α1-interacting domain (AID) in the I–II loop of $Ca_V2.2$. This amino acid has been shown both by the study that identified the AID motif and the recent structural studies to be key to the interaction between $Ca_V\beta$ subunits and the AID (Pragnell et al., 1994; Chen et al., 2004; Opatowsky et al., 2004; Van Petegem et al., 2004). This mutation prevents the enhancement of functional expression of $Ca_V2.2$ by $Ca_V\beta1b$ and also prevents modulation of $Ca_V2.2$ by this subunit. In addition, although the G-protein modulation of $Ca_V2.2W391A$ was present, it was not voltage dependent. In contrast, only the expression of the channel at the plasma membrane was affected when $Ca_V\beta2a$ was coexpressed with this mutant channel, whereas all of the biophysical properties of the expressed $Ca_V2.2W391A$ channels were still normally modulated by $Ca_V\beta2a$, including the voltage dependence of G-protein modulation. Our results further show that this was dependent on palmitoylation of $Ca_V\beta2a$ and suggest that the effect of $Ca_V\beta$ subunits on the voltage-dependent properties of the $Ca_V2.2$ channels occurs not only via the high-affinity I–II linker interaction but also via low-affinity interactions, presumably with other sites on the channel.

Materials and Methods

Materials. The cDNAs used in this study were $Ca_V2.2$ (D14157), $Ca_V\beta1b$ (X61394), $Ca_V\beta3$ (M88751), $Ca_V\beta2a$(M88751), $Ca_V\beta2a$-$\beta1b$ chimera (Olcese et al., 1994), α2δ-2 (Barclay et al., 2001), and D_2 dopamine receptor (X17458). The green fluorescent protein (GFP-mut3b, U73901) was used to identify transfected cells. All cDNAs were subcloned in pMT_2.

Construction, expression, and purification of proteins. $Ca_V2.2W391A$ was generated by site-directed mutagenesis with primers for $Ca_V2.2W391A.F$ (5′CGGGTACCTGGAGGCGATCTTCAAGGCTGAG) and $Ca_V2.2W391A.R$ (5′CTCAGCCTTGAAGATCGCCTCCAGGTACCCG).

$Ca_V2.2$ I–II loop in pGEX2T (Bell et al., 2001) [glutathione *S*-transferase (GST)-$Ca_V2.2$ I–II loop] was modified by PCR using *Pfu* polymerase (Stratagene, Amsterdam, The Netherlands) with the oligonucleotide primers 5′-ATGCTGGCCGAGGAGGACAGGAATGCAGAG-3′ and 5′-GACTCATTCCTCCGCCTTGAAGATCCACTCCAGGTAC-3′, which truncate the $Ca_V2.2$ I–II loop after the region encoding the AID. In this way, a construct was generated encoding the first 40 residues of the $Ca_V2.2$ I–II loop, incorporating the AID, fused to GST to form GST-$Ca_V2.2$(357–397)WT. Mutagenesis of GST-$Ca_V2.2$(357–397)WT was performed as described above using the primers 5′-ATCTTCAAGGCGGAGGAATGAGTCATGCTGGCCG-3′ and 5′-AGCCTCCAGGTACCCGTTGAGCTCTCGCTCGATC-3′ to substitute an alanine for W391. GST-$Ca_V2.2$(357–397)WT, GST-$Ca_V2.2$(357–397)W391A, and GST were expressed and purified as described for GST-$Ca_V2.2$ I–II loop by Bell et al. (2001). N-Terminally His-tagged $Ca_v\beta2a$ (H6N-$Ca_v\beta2a$) and C-terminally His-tagged $Ca_v\beta1b$ ($Ca_v\beta1b$-H6C) were expressed and purified as described by Bell et al. (2001).

Surface plasmon resonance. Assays were performed using a BIAcore 2000 (Biacore, Uppsala, Sweden) at 25°C using running buffer (20 mM Na phosphate, pH 7.5, 500 mM NaCl, and 0.005% Tween 20). Anti-GST monoclonal antibodies (Amersham Biosciences, Little Chalfont, UK) were covalently attached to the surface of CM5 dextran sensor chips according to the instructions of the manufacturer to allow the reversible immobilization of GST-fusion proteins. Approximately equivalent molar quantities ~350 resonance units (RU) of GST-$Ca_V2.2$(357–397)WT, ~350 RU of GST-$Ca_V2.2$(357–397)W391A, and ~300 RU of GST were immobilized on successive flow cells of a sensor chip. The flow rate of running buffer was 25 μl/min. H6N-$Ca_v\beta2a$ and $Ca_v\beta1b$-H6C were dialyzed against running buffer and diluted to a series of concentrations. These samples were applied for 6 min over all flow cells, and each injection was followed by a similar dissociation phase. The sensor chip surface was regenerated between injections by the application of 35 μl of 20 mM glycine/HCl, pH 2.2, at 10 μl/min and the immobilization of fresh ligand.

Sensorgrams were processed using the BIAevaluation 3.0 software (Biacore). Sensorgrams recorded from the flow cells containing GST-$Ca_V2.2$(357–397)WT and GST-$Ca_V2.2$(357–397)W391A were corrected for passive refractive index changes and for nonspecific interactions by subtraction of the corresponding sensorgram recorded from the flow cell containing GST only. Sensorgrams were fitted by nonlinear regression using Prism 4 (GraphPad Software San Diego, CA). For each sensorgram, the first 120 s of the association phase and the dissociation phase were fitted to a single exponential to determine the observed association rate $k_{on(obs)}$ and the dissociation rate k_{off}. The specific association rate, k_{on}, was calculated as $k_{on} = (k_{on(obs)} - k_{off})/[Ca_V\beta]$, and the dissociation constant K_D was calculated as $K_D = k_{off}/k_{on}$.

Cell culture and heterologous expression. The tsA-201 cells were cultured in a medium consisting of DMEM, 10% fetal bovine serum, and 1% nonessential amino acids. The cDNAs (all at 1 μg/μl) for $Ca_V\alpha1$ subunits, $Ca_V\beta$, $\alpha_2\delta$-2, D_2 dopamine receptor, and GFP (when used as a reporter of transfected cells) were mixed in a ratio of 3:2:2:2:0.4. The cells were transfected using Fugene6 (DNA/Fugene6 ratio of 2 μg in 3 μl; Roche Diagnostics, Lewes, UK). The tsA-201 cells were replated at low density on 35 mm tissue culture dishes on the day of recording.

Biotinylation. T75 flasks of transiently transfected tsA-201 cells were washed three times with 10 ml of PBS. Cells were incubated with 2 ml of PBS, pH 8.0, containing 800 μM EZ-link Sulfo NHS-SS-Biotin (Pierce, Rockford, IL) for 15 min at room temperature. The biotinylation reaction was terminated by addition of 10 ml of 100 mM glycine in PBS, and cells were collected by centrifugation (1000 × *g*) and washed an additional three times with 10 ml of PBS.

Cells were lysed by addition of 750 μl of lysis buffer (20 mM Tris, pH 7.4, 150 mM NaCl, 1 mM EDTA, and 1.5% Triton X-100) containing one Complete protease inhibitor tablet (Roche Diagnostics) per 10 ml, followed by brief sonication. After centrifugation at 20,000 × *g* for 20 min at 4°C, the protein concentration of the supernatant was determined using the BCA assay (Pierce). Biotinylated proteins were precipitated by incubating 500 μg of supernatant with 50 μl of streptavidin agarose beads (Pierce) for 3 h at room temperature. Precipitated proteins were washed four times with 1 ml of lysis buffer. Proteins were eluted from the beads by incubation with 100 mM dithiothreitol in lysis buffer for 30 min, followed by an equal volume of 2× SDS-PAGE sample buffer. Samples of supernatant and precipitated proteins were analyzed by SDS-PAGE on 4–12% Tris-glycine gels (Invitrogen, Paisley, UK) followed by Western blotting with anti $Ca_V2.2$ II–III linker antibodies (Raghib et al., 2001).

Western blot analysis. Samples (2.5–250 μg of protein) from tsA-201 whole-cell lysates [prepared as described for COS-7 cells by Raghib et al. (2001)] or from biotinylation experiments (see above) were separated by SDS-PAGE on 4–12% Tris-glycine gels and then transferred to polyvinylidene fluoride membranes. Immunodetection was performed with antibodies to the $Ca_v2.2$ II–III linker (Raghib et al., 2001) or β3 subunit (Canti et al., 2001) as described previously (Raghib et al., 2001).

Immunocytochemistry. Two days after transfection with $Ca_V\beta2a$ or $Ca_V\beta2aC3,4S$, tsA-201 cells were fixed with 4% paraformaldehyde in PBS for 5 min at room temperature. For permeabilization, cells were incubated twice for 7 min in a 0.02% solution of Triton X-100 in Tris-buffered saline. For detection of $Ca_V\beta2a$ or $Ca_V\beta2aC3,4S$, the primary antibody used was a rabbit anti-$Ca_V\beta2a$ (462–600) at 0.2 μg/ml (Chien et al., 1995). The secondary antibody was an anti-rabbit IgG FITC conjugated (1:500; Sigma, St. Louis, MO). For nuclear staining, 4′,6-diamidino-2-phenylindole (DAPI) (300 nM; Molecular Probes, Eugene, OR) was applied. Samples were mounted in VectaShield (Vector Laboratories, Burlingame, CA) to reduce photobleaching and examined on a confocal laser scanning microscope (model LSM; Ziess, Oberkochen, Germany) using a 40× objective (1.3 numerical aperture) with constant photomultiplier settings.

Whole-cell electrophysiology. Whole-cell patch-clamp recordings were performed at room temperature (22–24°C). Only fluorescent cells expressing GFP were used for recording. The single cells were voltage

clamped using an Axopatch 200B patch-clamp amplifier (Axon Instruments, Foster City, CA). The electrode potential was adjusted to give zero current between pipette and external solution before the cells were attached. The cell capacitance varied from 10 to 40 pF. Patch pipettes were filled with a solution containing the following (in mM): 140 Cs-aspartate, 5 EGTA, 2 $MgCl_2$, 0.1 $CaCl_2$, 2 K_2ATP, and 10 HEPES, titrated to pH 7.2 with CsOH (310 mOsm; with a resistance of 2–3 MΩ). The external solution contained the following (in mM): 150 tetraethylammonium bromide, 3 KCl, 1.0 $NaHCO_3$, 1.0 $MgCl_2$, 10 HEPES, 4 glucose, and 10 $BaCl_2$, pH adjusted to 7.4 with Tris base (320 mOsm). The pipette and cell capacitance as well as the series resistance were compensated by 80%. Leak and residual capacitance current were subtracted using a P/4 protocol. Data were filtered at 2 kHz and digitized at 5–10 kHz. The holding potential was −100 mV, and pulses were delivered every 10 s.

Data analysis and curve fitting. Current amplitude was measured 10 ms after the onset of the test pulse, and the average over a 2 ms period was calculated and used for subsequent analysis. The current density–voltage (*I–V*) relationships were fitted with a modified Boltzmann equation as follows: $I = G_{max} \times (V - V_{rev})/(1 + \exp(-(V - V_{50,\,act})/k))$, where I is the current density (in picoamperes per picofarad), G_{max} is the maximum conductance (in nanosiemens per picofarad), V_{rev} is the reversal potential, $V_{50,\,act}$ is the midpoint voltage for current activation, and k is the slope factor. Steady-state inactivation properties were measured by applying 5 s pulse from −120 to +20 mV in 10 mV increments, followed by a 11 ms repolarization to −100 mV before the 100 ms test pulse to +20 mV. Steady-state inactivation and activation data were fitted with a single Boltzmann equation of the following form: $I/I_{max} = (A_1 - A_2)/[1 + \exp((V - V_{50,\,inact})/k)] + A_2$, where I_{max} is the maximal current, and $V_{50,\,inact}$ is the half-maximal voltage for current inactivation. For the steady-state inactivation, A_1 and A_2 represent the proportion of inactivating and non-inactivating current, respectively. Inactivation kinetics of the currents were estimated by fitting the decaying part of the current traces with the following equation: $I(t) = C + A \times \exp(-(t - t_o)/\tau_{inact})$, where t_o is zero time, C the fraction of non-inactivating current, A the relative amplitude of the exponential, and τ_{inact} is its time constant. Activation kinetics were estimated by fitting the activation phase of the current with either a single or a double exponential. Analysis was performed using pClamp6 and Origin 7. Data are expressed as mean ± SEM of the number of replicates (n). Error bars indicate SEs of multiple determinations if not otherwise mentioned. Statistical significance was analyzed using Student's paired and unpaired t test, and $p < 0.05$ was considered to be statistically significant.

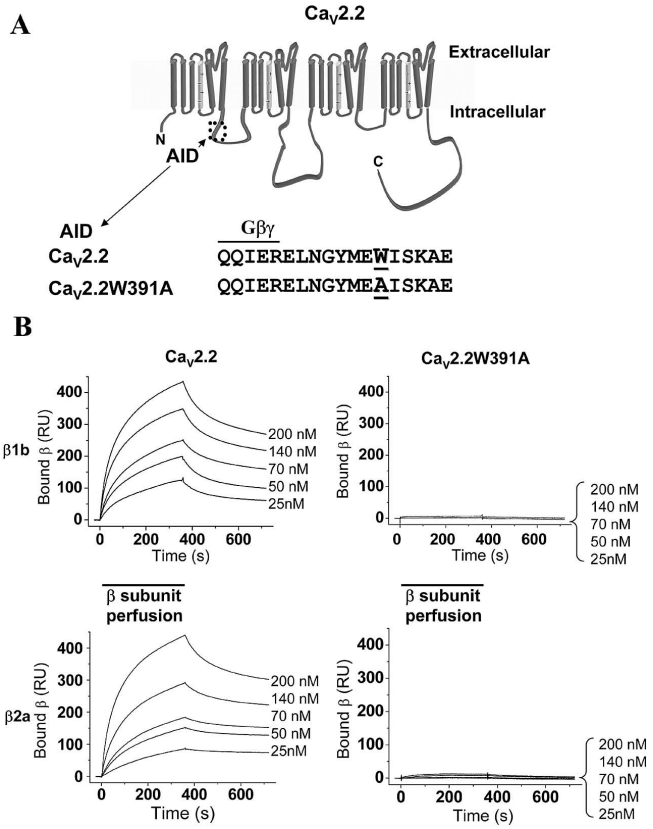

Figure 1. The W391A mutation prevents the binding of $Ca_V\beta1b$ and $Ca_V\beta2a$ to $Ca_V2.2$ I–II linker. ***A***, Representation of the $Ca_V2.2$ subunit that is composed of four domains of six transmembrane segments each. The I–II linker contains an 18 amino acid domain (AID) that interacts with $Ca_V\beta$ subunits (dotted box). The sequence of the AID within $Ca_V2.2$ and $Ca_V2.2W391A$ are given below, with W391 underlined and also showing the putative overlapping binding motif for $G\beta\gamma$ dimer binding. ***B***, Representative Biacore sensorgrams showing interactions between $Ca_V\beta1b$ (top) or $Ca_V\beta2a$ (bottom) with I–II loop GST-fusion proteins from $Ca_V2.2$ (left) and $Ca_V2.2W391A$ (right). The auxiliary $Ca_V\beta$ subunits (25–200 nM as indicated) were applied during the time indicated by the bars.

Results

Mutation of W391A in the I–II linker of $Ca_V2.2$ disrupts both $Ca_V\beta1b$ and $Ca_V\beta2a$ subunit binding

The amino acid W391 in $Ca_V2.2$ (Fig 1*A*) is conserved in the AID sequence of all HVA calcium channels (for review, see Dolphin, 2003a; Richards et al., 2004) and has been described previously to be important for the binding of the $Ca_V\beta$ ancillary subunits to HVA calcium channels (Pragnell et al., 1994; De Waard et al., 1996; Berrou et al., 2002). The recent structural analysis of the interaction of $Ca_V\beta$ subunits with the $Ca_V1.2$ I–II linker showed that this residue is deeply embedded in the AID binding groove in $Ca_V\beta$ (Chen et al., 2004; Opatowsky et al., 2004; Van Petegem et al., 2004). We first showed by surface plasmon resonance analysis that mutation of W391 to A in the AID of $Ca_V2.2$ prevents the binding of both $Ca_V\beta1b$ and $Ca_V\beta2a$ subunit to the I–II linker of $Ca_V2.2$ (Fig. 1*B*). In our experiments, GST-fusion proteins corresponding to the proximal I–II linker, including the AID of $Ca_V2.2$ or $Ca_V2.2W391A$, or GST alone as control, were immobilized via an anti-GST antibody to an individual flow cell of a CM5 dextran sensor chip. $Ca_V\beta$ subunit solutions (25–200 nM) were perfused over all flow cells. No binding of the $Ca_V\beta$ subunits to the control GST-fusion protein was detected (data not shown). $Ca_V\beta1b$ and $Ca_V\beta2a$ exhibited specific binding to the I–II linker of $Ca_V2.2$. From the data shown in Figure 1*B*, the dissociation constants (K_D) of $Ca_V\beta1b$ and $Ca_V\beta2a$ for the I–II loop of $Ca_V2.2$ were calculated to be 13.8 and 10.3 nM, respectively. Negligible binding of either $Ca_V\beta$ subunit was detected to the mutated $Ca_V2.2W391A$ I–II linker, and thus the K_D values could not be determined. We can only estimate that they must be at least 1000-fold less than for the I–II linker of the wild-type channel. From this assay, we show that the W391 present in the AID is crucial for the binding of $Ca_V\beta$ subunits to the proximal $Ca_V2.2$ I–II linker, and that the affinity for β binding to this construct is very similar to that observed previously for the full-length I–II linker (Bell et al., 2001).

$Ca_V\beta$ subunit binding is essential for functional expression of N-type calcium channels at the plasma membrane

Coexpression of $Ca_V2.2$ or $Ca_V2.2W391A$ with accessory $Ca_V\beta$ subunits allowed us to compare the biophysical properties of the wild-type and mutated channels. The $\alpha2\delta$-2 subunit was additionally present in all conditions in this study. The first striking effect of the W391A mutation was a large reduction of the current density for the mutated channel, consistent with a role of $Ca_V\beta$ binding to the I–II linker in trafficking Ca_V1 and Ca_V2 channels to the plasma membrane (Bichet et al., 2000) (Fig. 2*A*). The G_{max} determined from the *I–V* relationships for $Ca_V2.2W391A$ with

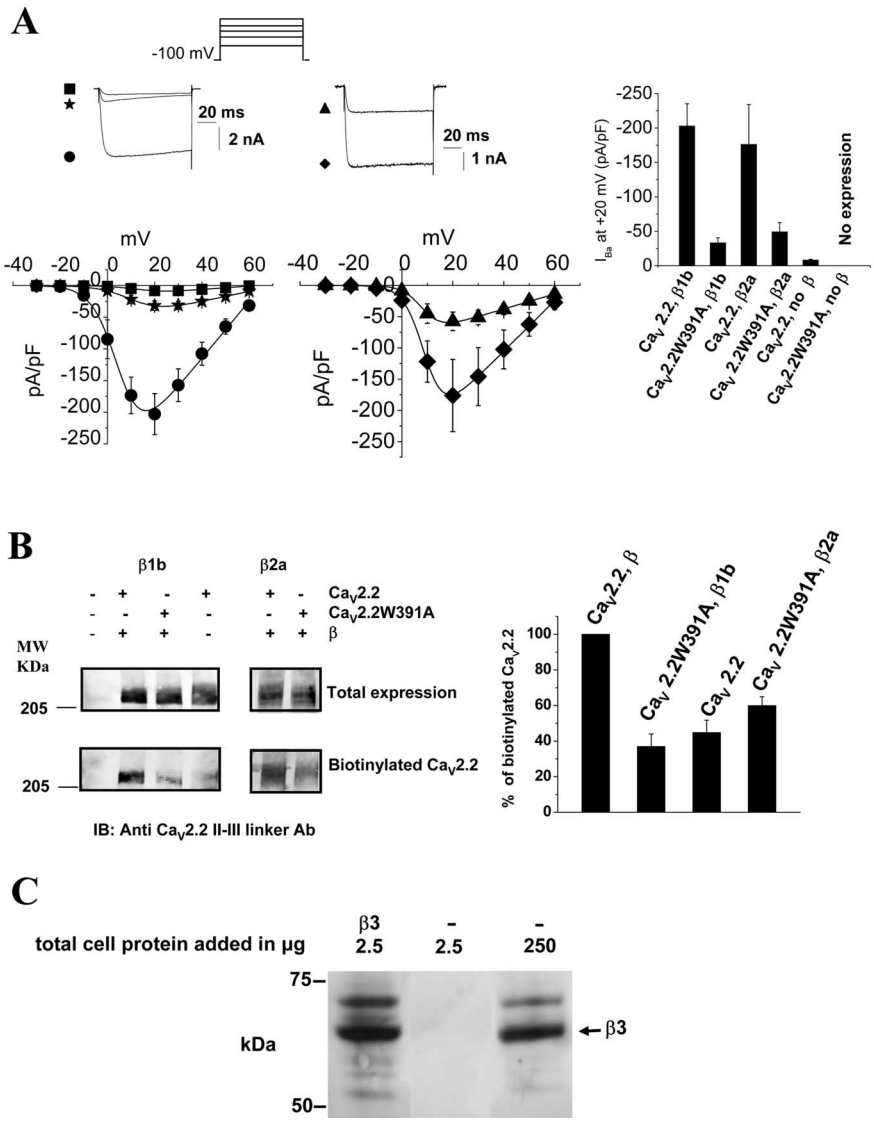

Figure 2. Role of $Ca_V\beta$ subunits in plasma membrane expression of $Ca_V2.2$. ***A***, Left, *I–V* relationships for $Ca_V2.2/\alpha2\delta$-2 coexpressed with $Ca_V\beta1b$ (filled circles, left; $n = 18$) or $Ca_V\beta2a$ (diamonds, right; $n = 13$) or without a $Ca_V\beta$ subunit (filled squares, left; $n = 13$) compared with *I–V* relationships for $Ca_V2.2W391A/\alpha2\delta$-2 coexpressed with $Ca_V\beta1b$ (filled stars, left; $n = 11$) or $Ca_V\beta2a$ (filled triangles, right; $n = 14$). The mean data are fitted with a modified Boltzmann function (see Materials and Methods), the $V_{50,\,act}$ and G_{max} values of which are given in Table 1. Typical Ba^{2+} current traces at +20 mV (identified by the symbols used) are shown above the *I–V* relationships. Right, Mean current density at +20 mV for each of these combinations ± SEM. ***B***, Cell surface expression of either $Ca_V2.2$ or $Ca_V2.2WA391A$ expressed with $\alpha2\delta$-2, either without $Ca_V\beta$ or with $Ca_V\beta1b$ (left) or with $Ca_V\beta2a$ (right). Total expression of $Ca_V2.2$ is shown by Western blot in the top row and biotinylated $Ca_V2.2$ in the bottom row. Cells were transfected with empty vector (lane 1), $Ca_V2.2/\alpha2\delta$-2/$\beta1b$ (lane 2), $Ca_V2.2W391A/\alpha2\delta$-2/$\beta1b$ (lane 3), $Ca_V2.2/\alpha2\delta$-2 (lane 4), $Ca_V2.2/\alpha2\delta$-2/$\beta2a$ (lane 5), or $Ca_V2.2W391A/\alpha2\delta$-2/$\beta2a$ (lane 6). Note that only the cell surface expression is affected similarly by the W391A mutation or by the absence of $Ca_V\beta$. Right, Histogram showing quantification of the mean amount of $Ca_V2.2WA391A$ expressed at the plasma membrane, when coexpressed with either $\beta1b$ or $\beta2a$, or $Ca_V2.2$ without $Ca_V\beta$, given as a percentage of the amount of $Ca_V2.2$ expressed with the relevant $Ca_V\beta$ present under the same conditions. Data are mean ± SEM of four independent experiments. MW, Molecular weight. ***C***, Western blot illustrating the endogenous expression of $Ca_V\beta3$ in tsA-201 cells. Gel loaded with 2.5 µg of protein prepared from cells transfected with $Ca_V\beta3$ (lane 1) compared with 2.5 or 250 µg of protein from cells transfected with an empty pMT2 vector (lanes 2, 3). An anti-$\beta3$ monoclonal antibody was used for immunoblotting.

$Ca_V\beta1b$ was significantly decreased by 81 ± 3% compared with the $Ca_V2.2/\beta1b$ combination (Fig. 2*A*; Table 1). The reduction in G_{max} was similar (94 ± 0.5%) when the wild-type channel was expressed in the absence of $Ca_V\beta$ (Fig. 2*A*; Table 1). Similarly, the G_{max} was decreased by 72 ± 6% for $Ca_V\beta2a$ with $Ca_V2.2W391A$ compared with the $Ca_V2.2/\beta2a$ combination (Fig. 2*A*; Table 1). In cells transfected with $Ca_V2.2W391A$ in the absence of a $Ca_V\beta$ subunit, none of the GFP-positive cells expressed any current ($n = 21$), whereas at least 90% of the GFP-positive $Ca_V2.2/\beta1b$-transfected cells displayed a current. This strongly suggests that $Ca_V2.2$ requires interaction via the I–II linker with a $Ca_V\beta$ to traffic to the plasma membrane.

We used a biotinylation assay to assess biochemically whether there were fewer channels present at the surface of the tsA-201 cells transfected with $Ca_V2.2W391A$ and a $Ca_V\beta$ subunit or when $Ca_V2.2$ was expressed without a $Ca_V\beta$ subunit, compared with wild-type $Ca_V2.2/Ca_V\beta$ combination. Whereas the total expression of $Ca_V2.2W391A$ was identical to the expression of $Ca_V2.2$ transfected with or without a $Ca_V\beta$, the amount of biotinylated channels at the plasma membrane was clearly lower (Fig. 2*B*). The W391A mutation decreased by 62 ± 5 and 37 ± 3% ($n = 4$) the number of channels that were present at the plasma membrane when coexpressed with $Ca_V\beta1b$ or $Ca_V\beta2a$, respectively. A similar diminution of the surface expression (by 52 ± 6%) was observed for the wild-type $Ca_V2.2$ when expressed without $Ca_V\beta$ (Fig. 2*B*). Even when the binding of $Ca_V\beta$ subunits to the proximal I–II linker, including the W391A AID, was negligible *in vitro*, some channels were still able to traffic to the plasma membrane. It is therefore possible that $Ca_V\beta$ subunits can bind to other binding sites present, for example, in the distal I–II linker or on the N and C terminus of the channel as suggested previously (Cornet et al., 2002; Maltez et al., 2005).

Given the foregoing results, the reason for the presence of a low level of wild-type $Ca_V2.2$ current in the absence of expressed $Ca_V\beta$ may therefore be the presence of an endogenous β subunit as described previously in *Xenopus* oocytes (Canti et al., 2001). This was examined by Western blotting using specific $Ca_V\beta$ antibodies. We clearly detected an endogenously expressed $Ca_V\beta3$ in tsA-201 cells (Fig. 2*C*). This endogenous $Ca_V\beta$ may be responsible for trafficking wild-type $Ca_V2.2$, allowing small currents to be recorded in cells transfected without $Ca_V\beta$ subunits, whereas the much lower affinity of the $Ca_V2.2W391A$ channel would preclude any interactions with the low level of endogenous $Ca_V\beta$.

Biophysical properties of $Ca_V2.2W391A$ expressed with $Ca_V\beta1b$ are similar to those of $Ca_V2.2$ expressed without $Ca_V\beta$

$Ca_V\beta1b$ is known to hyperpolarize the activation and the steady-state inactivation of HVA calcium channels (for review, see Dolphin, 2003a). If the W391A mutation were effectively disrupting

Table 1. Biophysical properties of $Ca_V2.2$ and $Ca_V2.2W391A$

	Maximum conductance (G_{max}, nS/pF)	Activation $V_{50,\,act}$ (*I–V* curves) (mV)	Activation $V_{50,\,act}$ (tail currents) (mV)	Inactivation $V_{50,\,inact}$ (mV)
No Ca_Vb				
$Ca_V2.2$	0.28 ± 0.01 *n* = 13	+14.8 ± 1.5	+24.8 ± 1.7 *n* = 8**	−35.1 ± 2.8 *n* = 6**
$Ca_V2.2W391A$	No expression *n* = 21			
$Ca_V\beta1b$				
$Ca_V2.2$	4.5 ± 0.2 *n* = 18	+5.2 ± 1.5	+13.6 ± 0.7 *n* = 19	−48.6 ± 2.2 *n* = 11
$Ca_V2.2W391A$	0.8 ± 0.02 *n* = 11**	+12.8 ± 2.1	+23.4 ± 1.4 *n* = 12**	−35.3 ± 3.5 *n* = 8**
$Ca_V\beta3$				
$Ca_V2.2$	2.9 ± 0.07 *n* = 7	+7.7 ± 0.3	N/D	−60.8 ± 0.7 *n* = 6
$Ca_V2.2W391A$	0.46 ± 0.03 *n* = 7**	+12.2 ± 0.9	N/D	−32.3 ± 1.6 *n* = 8**
$Ca_V\beta2a$				
$Ca_V2.2$	4.0 ± 0.09 *n* = 13	+9.3 ± 0.2	+20.4 ± 1.5 *n* = 10	+6.8 ± 2.3 *n* = 17
$Ca_V2.2W391A$	1.2 ± 0.04 *n* = 14*	+8.37 ± 0.3	+21 ± 1.5 *n* = 12	+6.2 ± 2.6 *n* = 18
$Ca_V\beta2aC3,4$				
$Ca_V2.2$	4.6 ± 0.2 *n* = 8	−1 ± 0.5	+9 ± 2.6 *n* = 10	−44.6 ± 0.4 *n* = 22
$Ca_V2.2W391A$	1.7 ± 0.07 *n* = 7*	+7.1 ± 0.7	+22.5 ± 2.5 *n* = 11**	−34.5 ± 3.2 *n* = 10*
$Ca_V\beta2a/\beta1b$				
$Ca_V2.2$	7.1 ± 0.3 *n* = 11	+4.9 ± 0.5	+19.4 ± 1.5 *n* = 14	−11.6 ± 2.5 *n* = 17
$Ca_V2.2W391A$	1.9 ± 0.08 *n* = 12**	+5.6 ± 0.5	+21.6 ± 1.6 *n* = 14	−17.5 ± 0.6 *n* = 17

Statistical significance of the indicated parameter was determined by unpaired *t* test, comparing data obtained for the wild-type $Ca_V2.2$ channels with $Ca_V2.2W391A$ when coexpressed without or with $Ca_V\beta$ subunits as indicated. *$p < 0.05$; **$p < 0.01$.

the binding of $Ca_V\beta1b$ to the channel, the biophysical properties of $Ca_V2.2W391A$ should be comparable with those of $Ca_V2.2$ expressed without any $Ca_V\beta$ subunit. This was indeed the case, because tail current analysis showed the $V_{50,\,act}$ to be depolarized by +9.8 and +11.2 mV, respectively, for $Ca_V2.2W391A/\beta1b$ and $Ca_V2.2$ in the absence of $Ca_V\beta$ compared with $Ca_V2.2/\beta1b$ (Fig. 3*A*,*B*; Table 1), confirming the $V_{50,\,act}$ estimates obtained from the *I–V* relationships (Table 1). This indicated that the W391A mutation abolished the effect of $Ca_V\beta1b$ on the voltage dependence of activation of $Ca_V2.2$, such that it behaved like the wild-type channel expressed without a $Ca_V\beta$ subunit.

Another important feature of $Ca_V\beta1$, $\beta3$, and $\beta4$ subunits is that they hyperpolarize the steady-inactivation curves of $Ca_V2.2$ as well as other HVA calcium channels (Bogdanov et al., 2000). The potential for half-inactivation ($V_{50,\,inact}$) was −48.6 mV for $Ca_V2.2$ expressed with $Ca_V\beta1b$ (Fig. 3*C*,*D*; Table 1). Again, in agreement with the assumption that the I–II linker of the $Ca_V2.2W391A$ channel does not bind $Ca_V\beta1b$, we found a significant depolarizing shift of the steady-state inactivation for $Ca_V2.2W391A/\beta1b$ [by +13 mV (Table 1)], whose steady-state inactivation curve is superimposed on that of $Ca_V2.2$ expressed without $Ca_V\beta1b$ (Fig. 3*C*,*D*; Table 1). $Ca_V\beta$ subunits are known to modulate not only the voltage dependence of the inactivation of calcium channels but also the kinetics of current decay (for review, see Dolphin, 2003a). The time constant of inactivation (τ_{inact}) of the $Ca_V2.2W391A/\beta1b$ current at +20 mV (209.2 ± 14.5 ms; $n = 14$) was smaller than that of the wild-type $Ca_V2.2/\beta1b$ combination (510.3 ± 51.6 ms; $n = 25$; $p < 0.01$), whereas the wild-type $Ca_V2.2$ expressed without a $Ca_V\beta$ subunit showed intermediate inactivation (Fig. 3*E*). The faster inactivation kinetics for the $Ca_V2.2W391A/\beta1b$ currents might be explained by the introduction of the mutation itself, because it has been shown previously that mutations in the AID are able to alter the inactivation kinetics (Dafi et al., 2004; Berrou et al., 2005).

Altogether, these results indicate that $Ca_V2.2W391A$ is not regulated by $Ca_V\beta1b$ in the plasma membrane. Furthermore, if, as our evidence suggests, $Ca_V2.2$ expressed without $Ca_V\beta$ subunit is trafficked to the plasma membrane by endogenous $Ca_V\beta$, this $Ca_V\beta$ does not regulate the channels once they have reached the membrane, as suggested previously (Canti et al., 2001).

Differential modulation of N-type channels by $Ca_V\beta2a$ subunits

Despite the fact that the W391A mutation effectively decreased the expression of $Ca_V2.2W391A$ channels at the plasma membrane in the presence of $Ca_V\beta2a$ as well as $Ca_V\beta1b$, no shift of activation was observed of the *I–V* curves when $Ca_V\beta2a$ was coexpressed with $Ca_V2.2W391A$ compared with the wild-type $Ca_V2.2/\beta2a$ combination (Fig. 2*A*). This was confirmed by analysis of tail currents. The $V_{50,\,act}$ was equivalent when either $Ca_V2.2$ or $Ca_V2.2W391A$ was coexpressed with $Ca_V\beta2a$ (Fig. 4*A*,*B*; Table 1).

As expected, $Ca_V\beta2a$ depolarized the $V_{50,\,inact}$ of $Ca_V2.2$ by +42 ± 2 mV compared with $Ca_V2.2$ expressed without $Ca_V\beta$ (Fig. 4*C*,*D*; Table 1). However, contrary to all expectations, we found that $Ca_V\beta2a$ was also able to depolarize the steady-state inactivation properties of $Ca_V2.2W391A$ to the same extent as for wild-type $Ca_V2.2$ (Fig. 4*D*; Table 1). Furthermore, $Ca_V\beta2a$ also slowed the inactivation kinetics of $Ca_V2.2W391A$ currents (Fig. 4*E*), abolishing the acceleration of the inactivation observed

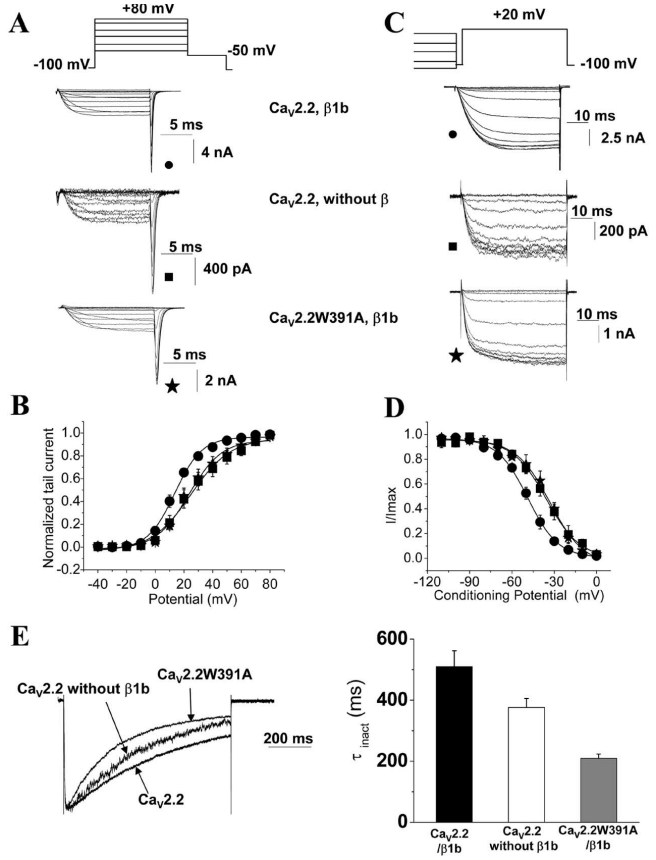

Figure 3. Biophysical properties of $Ca_V2.2$ and $Ca_V2.2W391A$ coexpressed with $Ca_V\beta1b$. ***A***, Representative current traces to illustrate current activation. Ba^{2+} tail currents were recorded after repolarizing to −50 mV after a 20 ms test pulse to between −40 and +80 mV from a holding potential of −100 mV. Top, $Ca_V2.2/\beta1b$; middle, $Ca_V2.2$ without any $Ca_V\beta$; bottom, $Ca_V2.2W391A/\beta1b$, all coexpressed with $\alpha2\delta$-2. ***B***, Voltage dependence of activation of $Ca_V2.2/\alpha2\delta$-2 coexpressed with $Ca_V\beta1b$ (filled circles) or without any $Ca_V\beta$ subunit (filled squares) or $Ca_V2.2W391A/\alpha2\delta$-2 expressed with $Ca_V\beta1b$ (filled stars). The normalized data, obtained from recordings such as those shown in ***A***, are plotted against the test pulse (n = 6–19). The mean data are fitted with a Boltzmann function, the $V_{50,\ act}$ values of which are given in Table 1. ***C***, Representative current traces (labeled as in ***A***) to illustrate steady-state inactivation protocols. Inward Ba^{2+} currents were recorded after conditioning pulses of 5 s duration, applied from a holding potential of −100 mV in 10 mV steps between −110 and +30 mV, followed by a 50 ms test pulse to +20 mV. ***D***, Voltage dependence of steady-state inactivation of $Ca_V2.2/\alpha2\delta$-2 coexpressed with $Ca_V\beta1b$ (filled circles) or without any $Ca_V\beta$ subunit (filled squares) or $Ca_V2.2W391A/\alpha2\delta$-2 expressed with $Ca_V\beta1b$ (filled stars). The normalized data obtained from recordings such as those shown in ***C*** are plotted against the conditioning potentials (n = 6–19). The mean data are fitted with a Boltzmann function, the $V_{50,\ inact}$ values of which are given in Table 1. ***E***, Left, Superposition of representative current traces for the subunit combinations indicated, recorded during an 800 ms depolarizing step to +20 mV, from a holding potential of −100 mV, normalized to the peak current. Right, Mean time constants of inactivation (τ_{inact}) obtained by fitting the decaying phase of the Ba^{2+} currents at +20 mV with a single exponential, for $Ca_V2.2/\alpha2\delta$-2/$\beta1b$ (black bar; n = 25), $Ca_V2.2/\alpha2\delta$-2 (white bar; n = 25), and $Ca_V2.2W391A/\alpha2\delta$-2/$\beta1b$ (gray bar; n = 14).

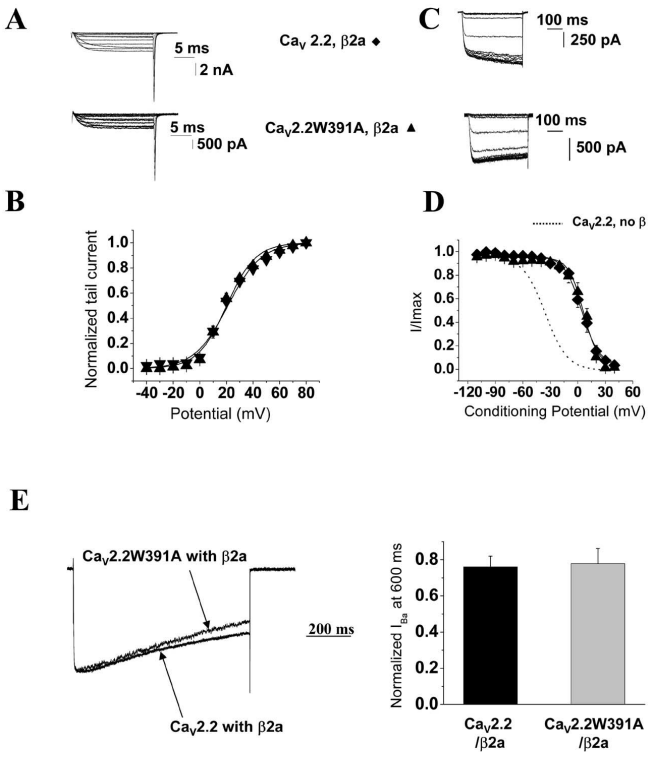

Figure 4. Biophysical properties of $Ca_V2.2$ and $Ca_V2.2WA391A$ coexpressed with $Ca_V\beta2a$. ***A***, Representative current traces to illustrate current activation using the same protocols as described in the legend to Figure 3. Top, $Ca_V2.2/\beta2a$; bottom, $Ca_V2.2W391A/\beta2a$, all coexpressed with $\alpha2\delta$-2. ***B***, Voltage dependence of activation for $Ca_V2.2/\alpha2\delta$-2 coexpressed with $Ca_V\beta2a$ (filled diamonds; n = 10) or $Ca_V2.2W391A/\alpha2\delta$-2 expressed with $Ca_V\beta2a$ (filled triangles; n = 12). The normalized data obtained from recordings such as those shown in ***A*** are plotted against the test pulse. The mean data are fitted with a Boltzmann function, the $V_{50,\ act}$ values of which are given in Table 1. ***C***, Representative current traces to illustrate steady-state inactivation using the same protocols as described in the legend to Figure 3. Top, $Ca_V2.2/\beta2a$; bottom, $Ca_V2.2W391A/\beta2a$. ***D***, Voltage dependence of steady-state inactivation for $Ca_V2.2/\alpha2\delta$-2 coexpressed with $Ca_V\beta2a$ (filled diamonds; n = 17) or $Ca_V2.2W391A/\alpha2\delta$-2 expressed with $Ca_V\beta2a$ (filled triangles; n = 18). The normalized data obtained from recordings such as those shown in ***C*** are plotted against the conditioning potentials. The mean data are fitted with a Boltzmann function, the $V_{50,\ inact}$ values of which are given in Table 1. The dotted line represents the fit for $Ca_V2.2$ without $Ca_V\beta$ from Figure 3*D*. ***E***, Left, Superposition of representative current traces for the subunit combinations indicated, recorded during an 800 ms depolarizing step to +20 mV, from a holding potential of −100 mV and normalized to the peak current. Right, Normalized residual I_{Ba} at 600 ms, for $Ca_V2.2/\alpha2\delta$-2/$\beta2a$ (black bar; n = 15) and $Ca_V2.2W391A/\alpha2\delta$-2/$\beta2a$ (gray bar; n = 14).

when $Ca_V2.2W391A$ was coexpressed with $Ca_V\beta1b$ (Fig. 3*E*), as noted previously for other mutations in the AID region (Dafi et al., 2004). The decay of the currents was <40% during the 800 ms depolarizing pulses and therefore could not be fitted with an exponential function, so we estimated the inactivation rate from the ratio of the current at 600 ms to that at the peak. The ratio at +20 mV was equivalent when $Ca_V\beta2a$ was coexpressed with either $Ca_V2.2$ (0.76 ± 0.06) or the mutated channel (0.77 ± 0.08) (Fig. 4*E*).

In summary, despite the fact that the W391 mutation was able to diminish the trafficking of the $Ca_V2.2W391A$ channels to the plasma membrane with all of the $Ca_V\beta$ subunits examined and in contrast to the results obtained for $Ca_V\beta1b$, the $Ca_V2.2W391A/\beta2a$ channels expressed at the cell surface were still modulated by $Ca_V\beta2a$.

Interaction with a $Ca_V\beta$ subunit is essential for the voltage dependence of the modulation of $Ca_V2.2$ calcium channels by G-protein activation

To investigate the importance of the W391 residue for the modulation by G-proteins of $Ca_V2.2$ calcium channels, we coexpressed a D_2 dopamine receptor with the $Ca_V2.2$, $Ca_V\beta1b$, $\alpha2\delta$-2 combination and activated the receptor with a maximal concentration (100 nM) of the agonist quinpirole. Figure 5*A* shows representative currents obtained before (P1) and immediately after (P2) a 100 ms depolarizing prepulse to +100 mV, before and during application of quinpirole. The currents measured at +10 mV were inhibited by quinpirole by 64.2 ± 4% for the wild-type

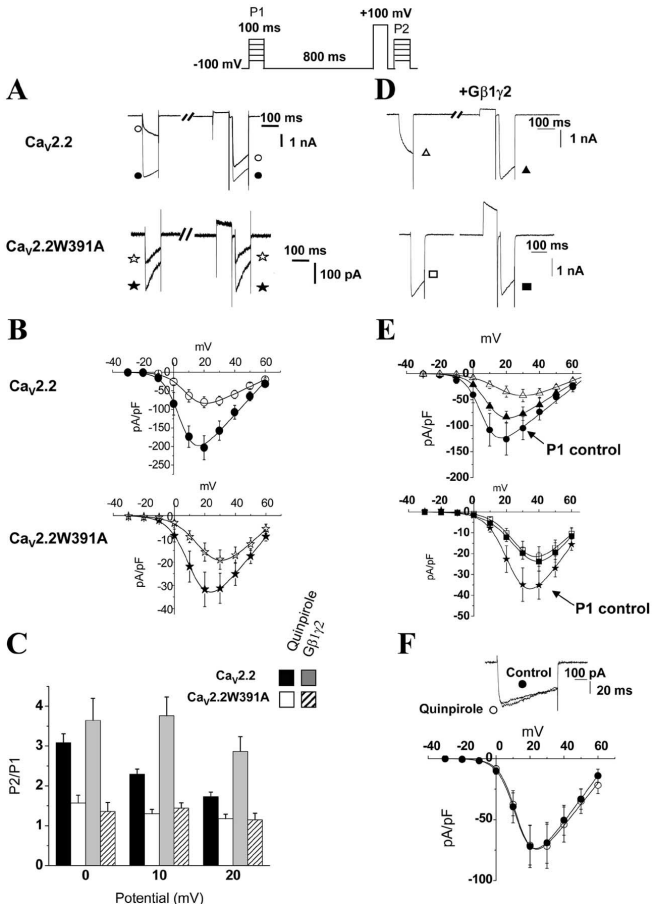

Figure 5. G-protein modulation of $Ca_V2.2$ and $Ca_V2.2W391A$ expressed with $Ca_V\beta1b$. Top, The pulse protocol used is depicted. A 100 ms test pulse (P1) from −30 to +60 mV was applied from a holding potential of −100 mV. After 800 ms repolarization to −100 mV, a 100 ms prepulse to +100 mV was applied. The cell was repolarized for 20 ms to −100 mV, and a second pulse (P2) identical to the first one was applied. ***A***, ***D***, Typical current traces obtained with this protocol are represented for $Ca_V2.2$ (top) and $Ca_V2.2W391A$ (bottom) coexpressed with $Ca_V\beta1b$. In ***A***, the D_2 dopamine receptor is coexpressed, and the top current traces (depicted by the open symbols) are in the presence of the agonist quinpirole (100 nM). In ***D***, $G\beta1\gamma2$ are coexpressed, and typical traces for $Ca_V2.2/\beta1b$ and $Ca_V2.2W391A/\beta1b$ are shown. ***B***, *I–V* curves for the calcium channel combinations are shown, obtained before (filled symbols) and during (open symbols) application of 100 nM quinpirole. Top, *I–V* curves for $Ca_V2.2/\alpha2\delta$-2 coexpressed with $Ca_V\beta1b$ (circles; $n = 18$) Bottom, *I–V* curves for $Ca_V2.2W391A/\alpha2\delta$-2 coexpressed with $Ca_V\beta1b$ (stars; $n = 11$) are represented. *I–V* curves are fitted with modified Boltzmann functions, the $V_{50,\,act}$ and G_{max} parameters of which are given in Table 1. ***E***, Top, *I–V* curves for Ba^{2+} currents during P1 for $Ca_V2.2/\alpha2\delta$-2/$\beta1b$ coexpressed without (filled circles; $n = 6$) or with (open triangles; $n = 9$) $G\beta1\gamma2$. Bottom, For $Ca_V2.2W391A/\alpha2\delta$-2/$\beta1b$ coexpressed without (stars; $n = 6$) or with (open squares; $n = 8$) $G\beta1\gamma2$. *I–V* curves obtained from currents recorded during P2 when $G\beta1\gamma2$ was coexpressed with $Ca_V2.2/\alpha2\delta$-2/$\beta1b$ (filled triangles; $n = 9$) or $Ca_V2.2W391A/\alpha2\delta$-2/$\beta1b$ (filled squares; $n = 8$) are also represented. All data were obtained in parallel on the same experimental days. ***C***, Voltage-dependent facilitation was calculated by dividing the peak current value obtained in P2 by that obtained in P1 at the potentials of 0, +10, and +20 mV, for $Ca_V2.2/\alpha2\delta$-2 with $Ca_V\beta1b$ (black bars; $n = 18$), $Ca_V2.2W391A/\alpha2\delta$-2 with $Ca_V\beta1b$ (white bars; $n = 11$) after application of quinpirole, or when $G\beta1\gamma2$ were coexpressed with $Ca_V2.2/\beta1b$ (gray bars; $n = 9$), $Ca_V2.2W391A/\beta1b$ (hatched bars; $n = 8$). ***F***, Typical current traces at +20 mV for R52,54A$Ca_V2.2W391A$ (top) coexpressed with $Ca_V\beta1b$ before (filled circles) and after (open circles) activation of the D_2 dopamine receptor. Corresponding *I–V* curves are represented in the bottom.

channel (Fig. 5*A*,*B*). The P2/P1 ratio obtained from traces such as those represented in Figure 5*A* reflects the voltage-dependent loss of inhibition. A value of 2.3 ± 0.1 ($n = 18$) was obtained for P2/P1 at +10 mV for the wild-type channel expressed with $Ca_V\beta1b$ (Fig. 5*C*).

For the $Ca_V2.2W391A/\beta1b$ currents, inhibition by quinpirole was similar, being 58.8 ± 5.2% at +10 mV ($n = 11$) (Fig. 5*A*,*B*). This inhibition was prevented by preincubating the cells for 16 h with 100 ng/ml pertussis toxin (PTX), as was inhibition of the wild-type currents (data not shown). However, the P2/P1 ratio was markedly diminished to 1.3 ± 0.1 at +10 mV ($n = 11$; $p < 0.01$) (Fig. 5*C*), demonstrating a lack of voltage-dependent loss of the G-protein modulation for the mutated channel. In agreement with this, when the $Ca_V2.2W391A/\beta1b$ combination was coexpressed with $G\beta1\gamma2$, it resulted in tonic inhibition compared with controls in the absence of $G\beta1\gamma2$, but these currents exhibited no slowed activation and no prepulse facilitation, in contrast to the wild-type $Ca_V2.2/\beta1b$ currents (Fig. 5*C–E*). Furthermore, although the $V_{50,act}$ of the *I–V* relationship was depolarized by +12.9 mV for the wild-type channel when $G\beta1\gamma2$ were cotransfected, it was only depolarized by +4.5 mV for the $Ca_V2.2W391A$ channels, in agreement with a reduced voltage dependence of the modulation by $G\beta\gamma$ of $Ca_V2.2W391A$ channels. Moreover, two arginines (R52 and R54) present in the N terminus of $Ca_V2.2$ are essential for the modulation by $G\beta\gamma$ of $Ca_V2.2$ calcium channels (Canti et al., 1999). After mutation of these two amino acids to alanines in the N terminus of $Ca_V2.2W391A$, quinpirole no longer inhibited the currents. This shows that these residues, and therefore $G\beta\gamma$, are involved in the voltage-independent inhibition of $Ca_V2.2W391A$ induced by activation of the D_2 dopamine receptor by quinpirole (Fig. 5*F*).

To investigate whether these data were contaminated by the increased inactivation rate of the $Ca_V2.2W391A/\beta1b$ combination compared with wild-type $Ca_V2.2/\beta1b$ currents, we also examined the quinpirole-mediated inhibition of the wild-type and mutated channels expressed with $Ca_V\beta3$, which produces more inactivation of wild-type $Ca_V2.2$ than does $Ca_V\beta1b$ (Fig. 6*A*). Unsurprisingly, when $Ca_V2.2W391A$ was coexpressed with $Ca_V\beta3$, the G_{max} was dramatically reduced by 83 ± 4% compared with wild-type $Ca_V2.2/\beta3$ (Fig. 6*A*; Table 1). There was also a +4.5 mV shift of the $V_{50,\,act}$ for $Ca_V2.2W391A$ compared with wild-type $Ca_V2.2/\beta3$, and the $Ca_V\beta3$ subunit did not hyperpolarize the steady-state inactivation of $Ca_V2.2W391A$ (Table 1). This suggests that, like $Ca_V\beta1b$, $Ca_V\beta3$ is not able to modulate the biophysical properties of $Ca_V2.2W391A$. However, quinpirole still inhibited $Ca_V2.2W391A/\beta3$ currents by 57.8 ± 11.8% at +10 mV ($p < 0.01$) (Fig. 6*A*). Furthermore, the voltage-dependent facilitation at +10 mV was greatly diminished from 2.5 ± 0.2 when $Ca_V\beta3$ was coexpressed with wild-type $Ca_V2.2$ to 1.3 ± 0.2 ($n = 7$; $p < 0.01$) for the $Ca_V2.2W391A/\beta3$ combination (Fig. 6*B*).

Although the $Ca_V2.2W391A$ currents exhibited faster inactivation kinetics than the wild-type currents, the decrease of facilitation observed for the $Ca_V2.2W391A$ currents was not attributable to inactivation occurring during either P1 or the prepulse, because the facilitation was similar for currents formed from $Ca_V2.2$ with either $Ca_V\beta1b$ or $Ca_V\beta3$, despite the fact that the latter showed accelerated inactivation kinetics (at +20 mV; τ_{inact} = 174.1 ± 17.1 ms; $n = 7$). In addition, at all prepulse durations from 5 to 200 ms, the P2/P1 ratio for the $Ca_V2.2W391A/\beta1b$ currents remained markedly reduced compared with $Ca_V2.2/\beta1b$ (Fig. 6*C*). Therefore, the inactivation occurring during the prepulse is not responsible for the apparent decrease in facilitation of $Ca_V2.2W391A$. Furthermore, the kinetics of facilitation could be fit to a single exponential, whose time constant (τ_{facil}) for $Ca_V2.2/\beta1b$ was 9.0 ± 1.4 ms (Fig. 6*C*), whereas the small residual facilitation was much slower for the $Ca_V2.2W391A/\beta1b$ combination

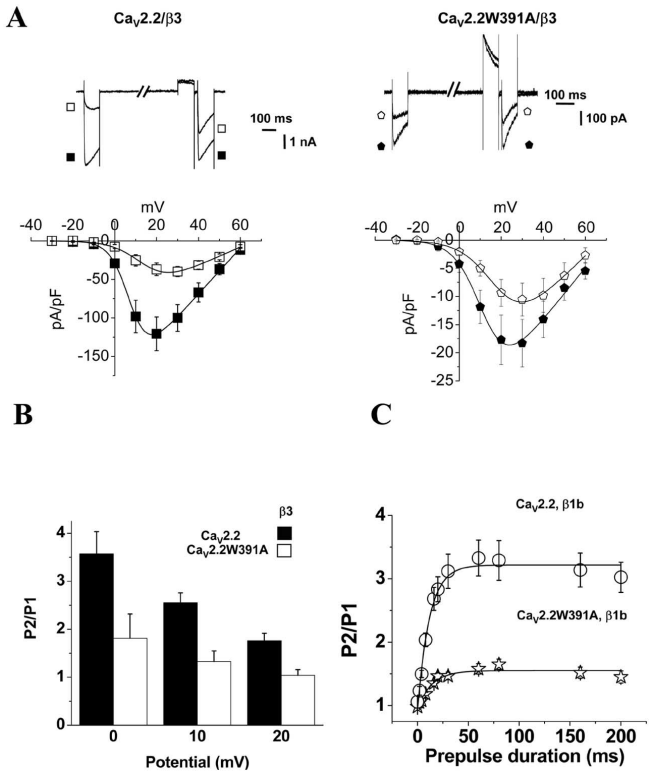

Figure 6. The kinetics of inactivation do not contaminate the properties of G-protein modulation of $Ca_V2.2$ and $Ca_V2.2W391A$. ***A***, Typical current traces obtained for $Ca_V2.2/\alpha2\delta$-2 and $Ca_V2.2W391A/\alpha2\delta$-2 coexpressed with $Ca_V\beta3$ and the D_2 dopamine receptor are represented (top). *I–V* curves obtained for these combinations before (filled symbols) and during (100 nM) application of quinpirole (open symbols) are also shown (bottom). ***B***, Voltage-dependent facilitation for $Ca_V2.2/\alpha2\delta$-2 (black bars; $n = 7$) or $Ca_V2.2W391A/\alpha2\delta$-2 coexpressed with $Ca_V\beta3$ (white bars; $n = 7$) obtained from the P2/P1 ratio when the D_2 dopamine receptor was activated by 100 nM quinpirole. ***C***, Facilitation rate of G-protein-modulated channels. The duration of the prepulse was increased from 0 to 200 ms. The P2/P1 facilitation ratios are given for each prepulse, for $Ca_V2.2$ (open circles; $n = 16$) and $Ca_V2.2W391A$ (open stars; $n = 17$) coexpressed with $Ca_V\beta1b$. Data are fitted with a single exponential, the time constant (τ_{facil}) of which is given in Results.

($\tau_{facil} = 16.7 \pm 3.2$ ms). These results indicate that $Ca_V\beta$ accelerates the kinetics of facilitation as described previously (Canti et al., 2000), but also that the presence of a $Ca_V\beta$ subunit, bound with high affinity to the I–II linker of $Ca_V2.2$, is essential for the voltage-dependent loss of inhibition, i.e., the ability of a +100 mV prepulse to remove G$\beta\gamma$-mediated inhibition in P2.

A related characteristic of the G-protein modulation of Ca_V2 channels is that the kinetics of current activation are slowed. Activation of the D_2 dopamine receptor significantly slowed the activation kinetics of $Ca_V2.2$ channels coexpressed with $Ca_V\beta1b$, increasing the time constant of activation (τ_{act}) from 2.0 ms to a combination of a similar fast $\tau_{act,fast}$ (2.2 ms) and a much slower $\tau_{act,slow}$ of 23.4 ms representing 36.5% of the current (Figs. 5*A*, 7*A*). In contrast, the activation kinetics for $Ca_V2.2W391A/\beta1b$ measured during a pulse to +10mV were unaffected by quinpirole. τ_{act} remained fast both before (2.1 ms) and during (2.1 ms) activation of the receptor (Figs. 5*A*, 7*A*).

Another hallmark of G-protein modulation is the depolarization of the voltage dependence of current activation. For the wild-type $Ca_V2.2$ coexpressed with $Ca_V\beta1b$, application of quinpirole induced a +17.5 mV shift of the $V_{50,act}$, from $+14.6 \pm 1.8$ to $+32.1 \pm 2.5$ mV ($n = 19$; $p < 0.01$) (Fig. 7*B*). This shift was reversible on washout of quinpirole (data not shown). There was no significant inhibition of tail current amplitude at +80 mV ($13.5 \pm 18.0\%$), indicating that all of the inhibition was entirely voltage dependent. In contrast, for $Ca_V2.2W391A$ coexpressed with $Ca_V\beta1b$, the tail currents were still significantly inhibited by $55.8 \pm 11.9\%$ at +80 mV ($p < 0.01$) (Fig. 7*B*). However, the $V_{50,act}$ for the residual $Ca_V2.2W391A/\beta1b$ was still depolarized by application of quinpirole by +14.9 mV, from $+27.5 \pm 3.7$ to $+42.4 \pm 1.9$ mV ($p < 0.01$) (Fig. 7*B*), as was also true for $Ca_V2.2$ expressed without a $Ca_V\beta$ subunit (data not shown), possibly indicating that G$\beta\gamma$ can still affect the voltage dependence of gating of $Ca_V2.2W391A$ by shifting the channel to a reluctant state. Altogether, these results strongly suggest that the loss of ability of $Ca_V2.2W391A$ to bind $Ca_V\beta1b$ was accompanied by the almost complete loss of voltage dependence of the G-protein modulation of N-type calcium channels.

$Ca_V2.2W391A$ coexpressed with $Ca_V\beta2a$ shows voltage-dependent G-protein modulation

When $Ca_V\beta2a$ was coexpressed with either $Ca_V2.2$ or $Ca_V2.2W391A$, quinpirole significantly inhibited the currents, by $64.4 \pm 6.2\%$ ($p < 0.01$) and $77.5 \pm 6.1\%$ ($p < 0.01$), respectively (Fig. 8*A*). Furthermore, in agreement with our evidence that $Ca_V2.2W391A$ was still associated with $Ca_V\beta2a$ (Fig. 4), we observed voltage-dependent facilitation of the $Ca_V2.2W391A/\beta2a$ combination, equivalent to that observed for the wild-type $Ca_V2.2/\beta2a$ (Fig. 8*A*,*B*). The P2/P1 ratio at +10 mV was 4.3 ± 0.6 for the wild-type channel and 3.7 ± 0.4 for $Ca_V2.2W391A$ (Fig. 8*B*).

For the $Ca_V2.2/\beta2a$ combination, τ_{act} was slowed by application of quinpirole from 2.2 ± 0.1 ms to a combination of a similar $\tau_{act,fast}$ (2.2 ms) and a very slow $\tau_{act,slow}$ (>400 ms), representing 51% of the current at 100 ms (Fig. 8*C*). The activation kinetics of $Ca_V2.2W391A$ were similarly slowed from a τ_{act} of 2.4 ± 0.1 ms to a combination of a similar $\tau_{act,fast}$ (2.4 ms) and a very slow $\tau_{act,slow}$ (>400 ms), representing 46% of the current at 100 ms (Fig. 8*C*). From tail currents recorded before and during activation of D_2 dopamine receptors, we observed an equivalent shift of $V_{50,act}$ of $+12.0 \pm 1.7$ and $+15.6 \pm 2.3$ mV for $Ca_V2.2$ and the mutated channel, respectively (Fig. 8*D*). At +80 mV, the control tail current amplitude was not significantly greater that that in the presence of quinpirole for $Ca_V2.2W391A/\beta2a$ (Fig. 8*D*), in contrast to the results obtained when $Ca_V\beta1b$ was coexpressed with $Ca_V2.2W391A$. We can conclude that $Ca_V\beta2a$ was still able to support voltage-dependent removal of the inhibition of $Ca_V2.2W391A$ induced by activation of the D_2 dopamine receptors.

Palmitoylation is responsible for the ability of $Ca_V\beta2a$ to regulate the voltage-dependent properties of $Ca_V2.2W391A$

A peculiarity of $Ca_V\beta2a$ is that it contains two cysteines in its N terminus that are palmitoylated. Palmitoylation of these residues strongly modulates the biophysical properties of calcium channels associated with $Ca_V\beta2a$, particularly their inactivation (Olcese et al., 1994; Chien et al., 1996; Qin et al., 1998; Bogdanov et al., 2000; Hurley et al., 2000; Restituito et al., 2000). To investigate the role of this palmitoylation, we used a $Ca_V\beta2a$ with the cysteines C3 and C4 mutated to serines ($Ca_V\beta2aC3,4S$) (Bogdanov et al., 2000) that is unable to incorporate palmitate (Qin et al., 1998). Coexpressing $Ca_V2.2$ with $Ca_V\beta2aC3,4S$ resulted in a significant hyperpolarization of the tail current $V_{50,act}$ by −11.4 mV compared with $Ca_V2.2/\beta2a$ (Fig. 9*A*; Table 1). The effect of $Ca_V\beta2aC3,4S$ was therefore similar to $Ca_V\beta1b$. In contrast, when

$Ca_V\beta$2aC3,4S was coexpressed with Ca_V2.2W391A, the voltage dependence of activation of the channel did not show any hyperpolarizing shift compared with Ca_V2.2W391A/β2a (Fig. 9*A*; Table 1), suggesting that, when not palmitoylated, the $Ca_V\beta$2aC3,4S subunit was not able to modulate the Ca_V2.2W391A channel.

As described previously (Qin et al., 1998; Bogdanov et al., 2000; Hurley et al., 2000; Restituito et al., 2000), coexpressing this mutated $Ca_V\beta$2aC3,4S subunit with Ca_V2.2 significantly hyperpolarized the steady-state inactivation compared with wild-type $Ca_V\beta$2a, by −51 mV (Fig. 9*B*; Table 1), and accelerated the kinetics of inactivation (Fig. 9*C*). In contrast, the steady-state inactivation $V_{50,\ inact}$ of the Ca_V2.2W391A channel coexpressed with $Ca_V\beta$2aC3,4S was significantly depolarized by >10 mV compared with the inactivation of the Ca_V2.2 channel in the presence of $Ca_V\beta$2aC3,4S (Fig. 9*B*; Table 1), suggesting a lack of modulation of Ca_V2.2W391A by $Ca_V\beta$2aC3,4S. As expected, currents recorded from cells expressing Ca_V2.2W391A with $Ca_V\beta$2aC3,4S also exhibited fast kinetics of inactivation, similar to those of this channel when coexpressed with $Ca_V\beta$1b (Fig. 9*C*).

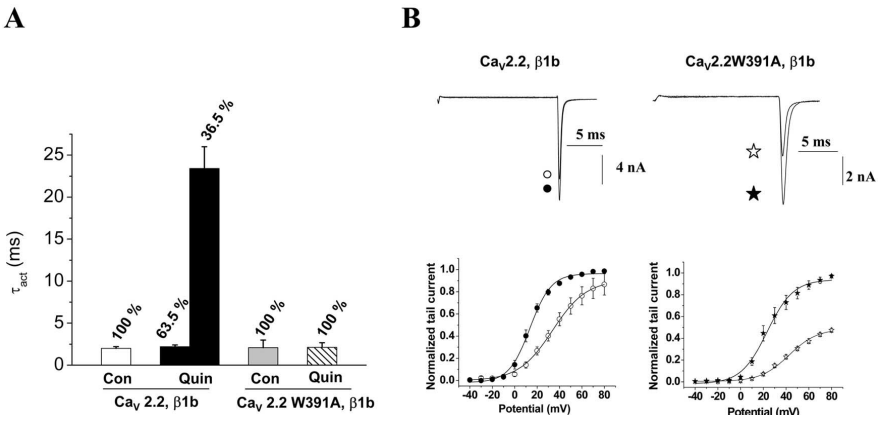

Figure 7. G-protein modulation of the kinetics and voltage dependence of activation of Ca_V2.2 and Ca_V2.2W391A coexpressed with β1b. ***A***, The τ_{act} for currents recorded in P1 as described in Figure 5 before and during perfusion of quinpirole in cells transfected with Ca_V2.2/α2δ-2/$Ca_V\beta$1b (white and black bars, respectively; $n = 18$) and with Ca_V2.2W391A/α2δ-2/β1b (gray and hatched bars, respectively; $n = 11$). For Ca_V2.2/α2δ-2/$Ca_V\beta$1b in the presence of quinpirole, the data were fit by a double exponential with a fast τ_{act} and a slow τ_{act}, the percentage of each component being given above the bars. ***B***, Activation curves derived from tail current amplitude measurements for Ca_V2.2/α2δ-2/β1b (left) and Ca_V2.2W391A/α2δ-2/β1b (right). Top, Typical tail current traces recorded after a test pulse to +80 mV before (filled symbols) and during (open symbols) application of 100 nM quinpirole. Bottom, Peak tail current density, before (filled symbols) and during (open symbols) application of quinpirole, for Ca_V2.2/α2δ-2/β1b (circles, left) or Ca_V2.2W391A/α2δ-2/β1b (stars, right). Data are the mean ± SEM of 12–19 cells, and the solid lines are Boltzmann functions fits, the parameters of which are given in Results.

We next determined whether the G-protein modulation of the wild-type Ca_V2.2/β2aC3,4S combination would be affected by the lack of palmitoylation of the $Ca_V\beta$ subunit. The currents in this case were still inhibited by 58.9 ± 2.6% ($n = 8$) (Fig. 9*D*), and the P2/P1 facilitation ratio was 3.5 ± 0.4 at +10 mV, comparable with that for the wild-type channel coexpressed with $Ca_V\beta$2a (Fig. 9*D*). However, when this mutated $Ca_V\beta$2aC3,4S was coexpressed with the mutated Ca_V2.2W391A, although the currents were still significantly inhibited by activation of the D_2 dopamine receptor by 61.4 ± 6.9% ($n = 7$) (Fig. 9*D*), the P2/P1 ratio was significantly diminished to 1.2 ± 0.7 at +10 mV (Fig. 9*D*). These results demonstrate that, when the W391A mutation in the I–II linker of Ca_V2.2 is accompanied by the mutation of the two palmitoylation sites in the N terminus of $Ca_V\beta$2a, it abolishes the ability of $Ca_V\beta$2a to support the voltage dependence of G-protein modulation of the channel. The lack of palmitoylation is confirmed by the altered distribution when expressed in tsA-201 cells, from wild-type $Ca_V\beta$2a being predominantly membrane associated to diffuse expression throughout the cytoplasm for $Ca_V\beta$2aC3,4S (Fig. 10*A*).

To confirm that this property was inherent to the palmitoylation of the $Ca_V\beta$ subunit, we used a chimera in which the N terminus of $Ca_V\beta$1b was swapped with that of $Ca_V\beta$2a to obtain a palmitoylatable $Ca_V\beta$1b (Olcese et al., 1994). The $Ca_V\beta$2a-β1b chimera was able to depolarize the $V_{50,act}$ of Ca_V2.2W391A currents (Fig. 9*A*), similar to $Ca_V\beta$2a. The chimeric $Ca_V\beta$2a-β1b subunit also significantly depolarized the steady-state inactivation of both the wild-type Ca_V2.2 channel and Ca_V2.2W391A by +37 and +17.8 mV, respectively, compared with channels containing the $Ca_V\beta$1b subunit with Ca_V2.2 or Ca_V2.2W391A (Fig. 9*B*; Table 1). Furthermore, the chimeric $Ca_V\beta$2a-β1b subunit slowed the inactivation of the wild-type channel and, to a lesser extent, the mutated Ca_V2.2W391A (Fig. 9*C*). Moreover, when coexpressed with $Ca_V\beta$2a-β1b, Ca_V2.2W391A currents were modulated by G-protein activation in a voltage-dependent manner (Fig. 9*D*). Ca_V2.2W391A exhibited prepulse facilitation during application of quinpirole; the P2/P1 ratio in this case was 3.0 ± 0.2, which was comparable with the value obtained for the wild-type channel expressed with $Ca_V\beta$2a-β1b (3.4 ± 0.2) (Fig. 9*D*). Altogether, these results show that the W391 is crucial for the voltage-dependent effects of $Ca_V\beta$1b and $Ca_V\beta$3 but not for those of palmitoylated $Ca_V\beta$2a, because palmitoylation of $Ca_V\beta$ can restore the voltage dependence of modulation of the mutated Ca_V2.2W391A channel.

Discussion

$Ca_V\beta$ subunits are membrane-associated guanylate-kinase proteins characterized by guanylate kinase-like (GK) domain that binds to the AID motif in the I–II loop of HVA Ca_Va1 subunits (Fig. 1*A*) and an Src homology 3 domain (SH3) (Hanlon et al., 1999). The 18 amino acid AID motif contains a conserved tryptophan that is crucial for binding $Ca_V\beta$ (Pragnell et al., 1994; Berrou et al., 2002). Recent structural data from three groups has provided detailed information about the interaction between the AID-$Ca_V\beta$ complex and confirmed that this tryptophan is deeply embedded in the binding groove within the GK of $Ca_V\beta$ (Chen et al., 2004; Opatowsky et al., 2004; Van Petegem et al., 2004).

Requirement of $Ca_V\beta$ for plasma membrane expression of HVA calcium channel

One of the main effects of $Ca_V\beta$ subunits on HVA calcium channels is to increase current density. However, the mechanism for this increase remains controversial, being attributed to increased trafficking (Bichet et al., 2000), increased maximum open probability (Neely et al., 2004), or both. Our data agree with previous studies showing biochemically that the amount of Ca_V1.2 channels in the plasma membrane was increased by $Ca_V\beta$ subunits (Altier et al., 2002; Cohen et al., 2005). We show that fewer channels are present at the surface when no $Ca_V\beta$ subunits were coexpressed or when the mutated Ca_V2.2W391A channels were cotransfected with a $Ca_V\beta$. It has been suggested that a $Ca_V\beta$ bound

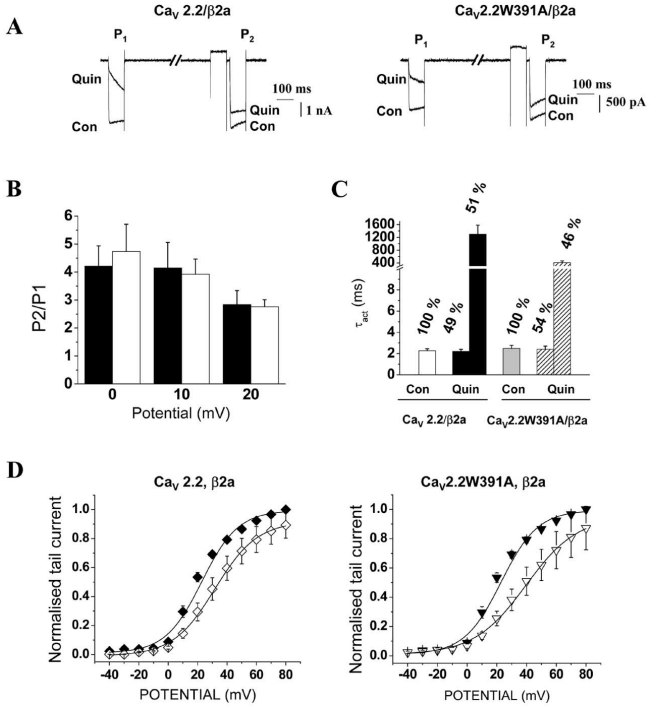

Figure 8. G-protein modulation of the kinetics and voltage dependence of activation of $Ca_V2.2$ and $Ca_V2.2W391A$ coexpressed with $Ca_V\beta2a$. ***A***, The effect of quinpirole (100 nM) is compared on the $Ca_V2.2/\alpha2\delta\text{-}2/\beta2a$ (left) and $Ca_V2.2W391A/\alpha2\delta\text{-}2/\beta2a$ (right) combinations. Representative currents traces using the P1/P2 pulse protocol shown in Figure 5, obtained before (Con) and during (Quin) application of 100 nM quinpirole. ***B***, The P2/P1 facilitation ratios for $Ca_V2.2/\alpha2\delta\text{-}2/\beta2a$ (black bars; $n = 13$) or $Ca_V2.2W391A/\alpha2\delta\text{-}2/\beta2a$ (white bars; $n = 14$) at potentials between 0 and +20 mV are given. ***C***, The τ_{act} values for currents activated by +20 mV steps before and during application of quinpirole. Values are given for $Ca_V2.2/\alpha2\delta\text{-}2/\beta2a$ in control conditions (white bars) and in the presence of quinpirole (black bars; $n = 13$) or for the $Ca_V2.2W391A$ (gray and hatched bars, respectively; $n = 14$). In the presence of quinpirole, the data were fit by two exponentials, with the percentage of the total represented by each component given above the bar. ***D***, Activation derived from normalized tail current density before (filled symbols) and during (open symbols) application of quinpirole (100 nM) for the subunit combination $Ca_V2.2/\alpha2\delta\text{-}2/\beta2a$ (left, diamonds; $n = 10$) or $Ca_V2.2W391A/\alpha2\delta\text{-}2/\beta2a$ (right, triangles; $n = 12$). The solid lines are Boltzmann function fits to the mean data, the parameters of which are given in Results.

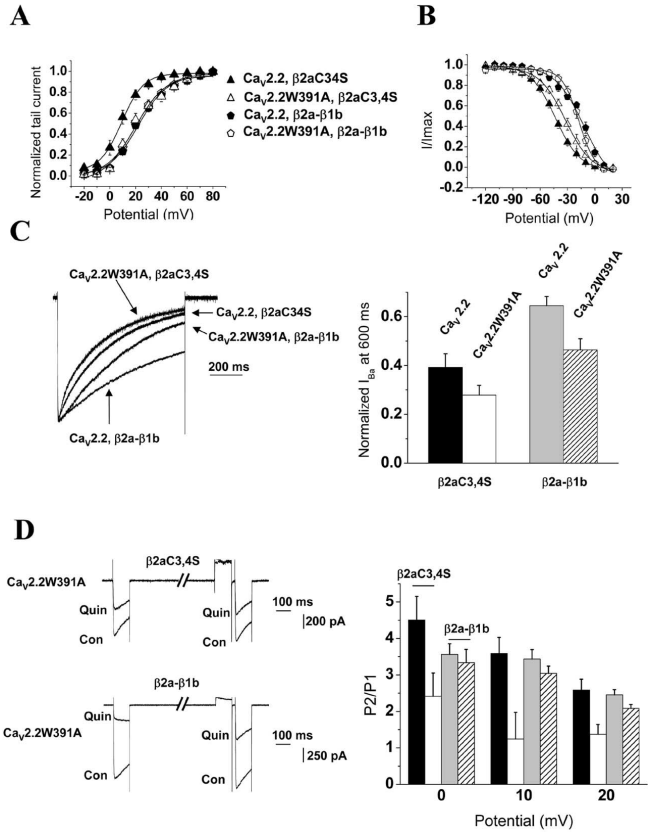

Figure 9. Effect of palmitoylation of $Ca_V\beta$ subunits on the modulation of $Ca_V2.2$ and $Ca_V2.2W391A$ channels. ***A***, Voltage dependence of activation of $Ca_V2.2$ (filled symbols) or $Ca_V2.2W391A$ (open symbols) with either $Ca_V\beta2aC3,4S$ (triangles) or $Ca_V\beta2a\text{-}\beta1b$ chimera (pentagons) and $\alpha2\delta\text{-}2$. The solid lines are Boltzmann function fits to the mean data, the parameters of which are given in Results. ***B***, Voltage dependence of steady-state inactivation of $Ca_V2.2$ (filled symbols) or $Ca_V2.2W391A$ (open symbols) with either $Ca_V\beta2aC3,4S$ (triangles) or $Ca_V\beta2a\text{-}\beta1b$ chimera (pentagons) and $\alpha2\delta\text{-}2$. The solid lines are Boltzmann function fits to the mean data, the parameters of which are given in Results. ***C***, Left, Representative Ba^{2+} current traces recorded during an 800 ms depolarizing step to +20 mV from a holding potential of −100 mV. Right, The normalized amount of residual current at 600 ms, obtained for $Ca_V2.2$ or $Ca_V2.2W391A$ coexpressed with $\alpha2\delta\text{-}2$ and $Ca_V\beta2aC3,4S$ (black and white bars, respectively; $n = 18$ for both) or the $Ca_V\beta2a\text{-}\beta1b$ chimera (gray and hatched bars; $n = 23$ and $n = 19$, respectively). ***D***, Left, The effect of quinpirole (100 nM) is compared for the subunit combinations $Ca_V2.2W391A/\alpha2\delta\text{-}2/\beta2aC3,4S$ (top traces) and $Ca_V2.2W391A/\alpha2\delta\text{-}2/\beta2a\text{-}\beta1b$ chimera (bottom traces). Representative currents traces using the P1/P2 pulse protocol shown in Figure 5, obtained before (Con) and during (Quin) application of 100 nM quinpirole. Right, The P2/P1 ratio obtained from such traces for $Ca_V2.2$ and $Ca_V2.2W391A$ coexpressed with $\alpha2\delta\text{-}2$ and $Ca_V\beta2aC3,4S$ (black and white bars; $n = 7$ and $n = 8$, respectively) or the $Ca_V\beta2a\text{-}\beta1b$ chimera (gray and hatched bars; $n = 12$ and $n = 11$ respectively).

to the I–II linker may mask an endoplasmic reticulum (ER) retention signal present in the I–II linker of HVA calcium channels and favor the trafficking of the channel to the cell surface (Bichet et al., 2000). If the trafficking of the channel were the only process affected by the lack of a $Ca_V\beta$ bound to the I–II linker of $Ca_V2.2$, the reduction of the current density, as judged by the G_{max}, and the amount of $Ca_V2.2$ expressed at the plasma membrane would be the same. However, the G_{max} was more affected than the plasma membrane expression of $Ca_V2.2$ (81 and 62% reduction, respectively, when coexpressed with $Ca_V\beta1b$). The reason for this is likely to be that $Ca_V\beta$ not only traffics the channel to the surface but also increases the maximum open probability of the channel, as suggested previously (Wakamori et al., 1999; Meir et al., 2000; Neely et al., 2004).

When no $Ca_V\beta$ was coexpressed with wild-type $Ca_V2.2$ channels, small currents remained, whereas none of the GFP-positive cells transfected with the mutated $Ca_V2.2W391A$ channel alone expressed any current. This suggests that the endogenous $Ca_V\beta3$ that we have identified in tsA-201 cells was responsible for trafficking some wild-type $Ca_V2.2$ to the plasma membrane, and that the markedly reduced affinity of the W391A mutated channel for $Ca_V\beta$ subunits prevented interaction with the endogenous $Ca_V\beta3$ subunits and thus their trafficking to the plasma membrane. When a $Ca_V\beta$ subunit was cotransfected with $Ca_V2.2W391A$ channel, a small fraction of these channels were then trafficked to the plasma membrane, presumably because the overexpressed $Ca_V\beta$ was able to either bind with low affinity to the mutated I–II linker of $Ca_V2.2W391A$ or mask other ER retention signals that may be present on other parts of the channel (Cornet et al., 2002). Our results therefore provide very strong evidence that the binding of a $Ca_V\beta$ auxiliary subunit to the channel is an essential requirement for functional expression of $Ca_V2.2$ at the plasma membrane.

Role of $Ca_V\beta$ in voltage-dependent modulation of N-type calcium channels

Apart from their important role in trafficking, $Ca_V\beta$ subunits also modify the biophysical properties of calcium channels (for re-

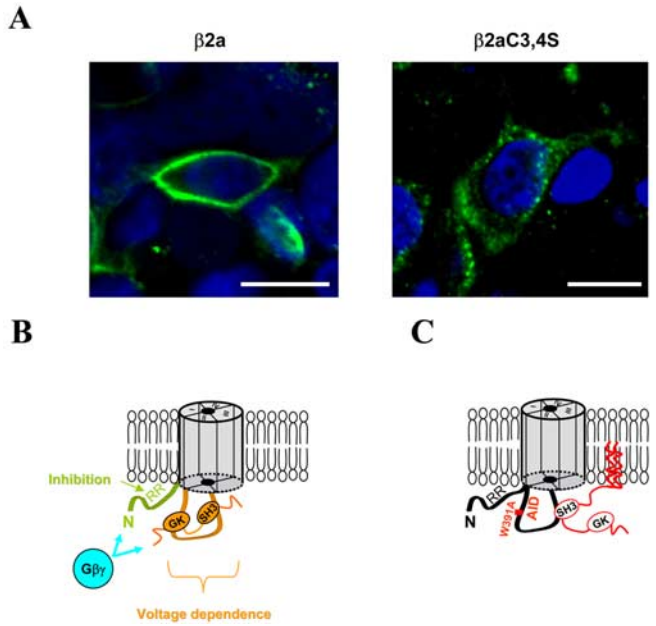

Figure 10. Proposed mechanism for G-protein modulation of $Ca_V2.2$ calcium channels and the effect of palmitoylation on the interaction of $Ca_V\beta$ subunits with the I–II linker. ***A***, Confocal immunofluorescent images of β2a and β2aC3,4S subunits expressed in tsA-201 cells, using an anti-β2 antibody (green). Nuclei are visualized with DAPI (blue). Scale bars, 20 μm. Note the membrane localization of the β2a subunit (left), whereas the β2aC3,4S subunit is localized to the cytoplasm (right). ***B***, Model for the mechanism of action of Gβγ binding to the channel to inhibit its activity. The N terminus of $Ca_V2.2$ containing two arginines (R52, R54) constitutes a motif implicated in the inhibition by G-proteins, whereas the voltage-dependent facilitation (loss of inhibition induced by strong depolarization) requires a bound $Ca_V\beta$ subunit on the I–II linker. ***C***, The GK domain of $Ca_V\beta$ subunits interacts with the AID, allowing a low-affinity binding of its SH3 domain elsewhere on the channel (e.g., to the I–II loop of $Ca_V2.2$) (Maltez et al., 2005) to modulate the properties of the channel. Palmitoylation of $Ca_V\beta$ by anchoring the subunit to the plasma membrane allows this low-affinity interaction to occur when the W391 in the AID is mutated to disrupt its interaction with the GK domain.

view, see Dolphin, 2003a). Despite our conclusion that interaction with $Ca_V\beta$ (either endogenous or expressed) is essential for trafficking to the plasma membrane, when $Ca_V2.2$ was expressed alone, its activation and inactivation properties were shifted to more positive potentials compared with those for $Ca_V2.2$ coexpressed with $Ca_V\beta1b$ or $Ca_V\beta3$. The $Ca_V2.2W391A/\beta1b$ or $Ca_V\beta3$ combinations showed similar biophysical properties to wild-type $Ca_V2.2$ channels expressed without a $Ca_V\beta$. Thus, although the channels required a $Ca_V\beta$ to be trafficked to the plasma membrane, they were not modulated by the $Ca_V\beta$ subunits when inserted in the plasma membrane, in agreement with our previous results suggesting two binding sites with differing affinities (Canti et al., 2001).

G-protein modulation of $Ca_V2.2$ calcium channels requires $Ca_V\beta$ subunits to exhibit voltage dependence

Another unexpected feature of our results was that the $Ca_V2.2W391A/\beta1b$ currents were still inhibited by D_2 dopamine receptor activation to the same extent as wild-type $Ca_V2.2$ channels, although there was no voltage-dependent relief of this inhibition. In our experiments, maximal inhibition of the $Ca_V2.2W391A/\beta1b$ currents remained fast, occurring within <10 s, and was PTX sensitive. Furthermore, $Ca_V2.2W391A/\beta1b$ currents were also tonically inhibited by Gβγ in a voltage-independent manner. We suggest that Gβγ dimers are involved both in the voltage-independent modulation of $Ca_V2.2W391A/\beta1b$ currents and in the voltage-dependent modulation of the wild-type $Ca_V2.2$ currents.

Two models have been proposed for the regulation of HVA calcium channels by G-proteins. In the first, Gβγ dimers displace $Ca_V\beta$ from the I–II loop, resulting in the reluctant state (Sandoz et al., 2004), whereas in the second model, both Gβγ and $Ca_V\beta$ subunits would be able to bind to the channel at the same time (Meir et al., 2000; Hummer et al., 2003; Richards et al., 2004), with Gβγ binding producing the reluctant state. In the present study, the fact that activating the D_2 dopamine receptor still leads to a large inhibition of $Ca_V2.2W391A$ currents also suggests that the Gβγ has direct effects on channel gating and does not simply displace $Ca_V\beta$ subunits. Moreover, Van Petegem et al. (2004) speculated that, because the Gβγ–AID affinity is at least 10- to 20-fold weaker than the $Ca_V\beta$–AID affinity and a major conformational change would be required for Gβγ to displace $Ca_V\beta$, this was unlikely to occur (Van Petegem et al., 2004).

We showed previously that two arginines in the N terminus of Ca_V2 calcium channels are critical for G-protein modulation (Canti et al., 1999). By mutating these residues in the N terminus of $Ca_V2.2W391A$, we demonstrate that they are also critical for the voltage-independent inhibition of the $Ca_V2.2W391A$ channel, whereas the voltage-dependent removal of this inhibition, or facilitation, involving the unbinding of Gβγ requires $Ca_V\beta$ to be bound to the I–II linker of the channel (Fig. 10*B*), as suggested previously (Meir et al., 2000).

Palmitoylation of $Ca_V\beta2a$ subunits allows its interaction with $Ca_V2.2W391A$

Unlike other $Ca_V\beta$ subunits, palmitoylated $Ca_V\beta2a$ depolarizes, rather than hyperpolarizes, the steady-state inactivation of HVA calcium channels (Jones et al., 1998; Restituito et al., 2000). This observation led to the conclusion that the I–II linker might constitute the inactivation gate of HVA calcium channels, with its mobility being reduced by the palmitoylation of $Ca_V\beta2a$ anchoring it to the plasma membrane (Restituito et al., 2000). In our study, the $Ca_V2.2W391A$ channels trafficked to the plasma membrane by $Ca_V\beta2a$ remained modulated by this subunit, in contrast to $Ca_V\beta1b$, and our evidence shows clearly that this is attributable to the palmitoylation of $Ca_V\beta2a$. The mutated $Ca_V\beta C3,4S$ subunit was not able to modulate the biophysical properties of the $Ca_V2.2W391A$ channels, demonstrating that palmitoylation of $Ca_V\beta2a$ helps to anchor the subunit to the channel. This hypothesis was confirmed by creating a palmitoylatable $Ca_V\beta1b$ that was able to modulate the biophysical properties of the $Ca_V2.2W391A$ channel.

As shown recently (Cohen et al., 2005; Maltez et al., 2005) and confirmed here, the AID–GK interaction is essential to traffic the channels to the plasma membrane. Our data suggest that either this interaction is not promoted by palmitoylation of $Ca_V\beta2a$ or $Ca_V\beta2a$ is not palmitoylated during the trafficking process, until the $Ca_V2.2/\beta2a$ complex is inserted in the plasma membrane.

Short $Ca_V\beta$ subunits that lack the GK domain retain the ability to modulate the open probability of $Ca_V1.2$, suggesting another low-affinity binding site on the Ca_V subunit for the SH3 domain (Cohen et al., 2005). An interaction of the SH3 with the I–II linker has been then demonstrated that modulates biophysical properties of calcium channels such as their inactivation (Maltez et al., 2005). The authors suggest that the role of the

high-affinity GK–AID interaction is to increase the local concentration of $Ca_V\beta$ and to promote lower-affinity interactions. In a similar way, palmitoylation of $Ca_V\beta$2a, promoting its membrane localization (Fig. 10*A*) and thus increasing its local concentration, may allow its binding to the Ca_V2.2W391A channel via interaction with low-affinity binding sites, such as the C and N termini or other sites on the I–II linker (Fig. 10*C*), that might be critical for the voltage-dependent properties of the channel, including the voltage dependence of G-protein modulation (Walker et al., 1999; Stephens et al., 2000; Maltez et al., 2005).

We also show here that, despite differentially affecting the biophysical properties of calcium channels, $Ca_V\beta$1b and $Ca_V\beta$2a subunits play the same role in the voltage dependence of G-protein modulation. They are necessary for voltage-dependent facilitation presumably via the second low-affinity site. Our results therefore show conclusively that $G\beta\gamma$ dimers have a direct inhibitory effect on Ca_V2.2 channel gating, and that $Ca_V\beta$ subunits are required for the voltage-dependent removal of this inhibition.

References

Altier C, Dubel SJ, Barrere C, Jarvis SE, Stotz SC, Spaetgens RL, Scott JD, Cornet V, De Waard M, Zamponi GW, Nargeot J, Bourinet E (2002) Trafficking of L-type calcium channels mediated by the postsynaptic scaffolding protein AKAP79. J Biol Chem 277:33598–33603.

Barclay J, Balaguero N, Mione M, Ackerman SL, Letts VA, Brodbeck J, Canti C, Meir A, Page KM, Kusumi K, Perez-Reyes E, Lander ES, Frankel WN, Gardiner RM, Dolphin AC, Rees M (2001) Ducky mouse phenotype of epilepsy and ataxia is associated with mutations in the *Cacna2d2* gene and decreased calcium channel current in cerebellar Purkinje cells. J Neurosci 21:6095–6104.

Bean BP (1989) Neurotransmitter inhibition of neuronal calcium currents by changes in channel voltage dependence. Nature 340:153–156.

Bell DC, Butcher AJ, Berrow NS, Page KM, Brust PF, Nesterova A, Stauderman KA, Seabrook GR, Nurnberg B, Dolphin AC (2001) Biophysical properties, pharmacology, and modulation of human, neuronal L-type (α1D, Ca_V1.3) voltage-dependent calcium currents. J Neurophysiol 85:816–827.

Berrou L, Klein H, Bernatchez G, Parent L (2002) A specific tryptophan in the I-II linker is a key determinant of β-subunit binding and modulation in Ca_V2.3 calcium channels. Biophys J 83:1429–1442.

Berrou L, Dodier Y, Raybaud A, Tousignant A, Dafi O, Pelletier JN, Parent L (2005) The C-terminal residues in the alpha-interacting domain (AID) helix anchor $Ca_V\beta$ subunit interaction and modulation of Ca_V2.3 channels. J Biol Chem 280:494–505.

Bichet D, Cornet V, Geib S, Carlier E, Volsen S, Hoshi T, Mori Y, De Waard M (2000) The I-II loop of the Ca^{2+} channel α1 subunit contains an endoplasmic reticulum retention signal antagonized by the β subunit. Neuron 25:177–190.

Bogdanov Y, Brice NL, Canti C, Page KM, Li M, Volsen SG, Dolphin AC (2000) Acidic motif responsible for plasma membrane association of the voltage-dependent calcium channel β1b subunit. Eur J Neurosci 12:894–902.

Canti C, Page KM, Stephens GJ, Dolphin AC (1999) Identification of residues in the N terminus of α1B critical for inhibition of the voltage-dependent calcium channel by $G\beta\gamma$. J Neurosci 19:6855–6864.

Canti C, Bogdanov Y, Dolphin AC (2000) Interaction between G proteins and accessory subunits in the regulation of α1B calcium channels in *Xenopus* oocytes. J Physiol (Lond) 527:419–432.

Canti C, Davies A, Berrow NS, Butcher AJ, Page KM, Dolphin AC (2001) Evidence for two concentration-dependent processes for beta-subunit effects on α1B calcium channels. Biophys J 81:1439–1451.

Catterall WA (2000) Structure and regulation of voltage-gated Ca^{2+} channels. Annu Rev Cell Dev Biol 16:521–555.

Chen YH, Li MH, Zhang Y, He LL, Yamada Y, Fitzmaurice A, Shen Y, Zhang H, Tong L, Yang J (2004) Structural basis of the α1-β subunit interaction of voltage-gated Ca^{2+} channels. Nature 429:675–680.

Chien AJ, Zhao X, Shirokov RE, Puri TS, Chang CF, Sun D, Rios E, Hosey MM (1995) Roles of a membrane-localized beta subunit in the formation and targeting of functional L-type Ca^{2+} channels. J Biol Chem 270:30036–30044.

Chien AJ, Carr KM, Shirokov RE, Rios E, Hosey MM (1996) Identification of palmitoylation sites within the L-type calcium channel β2a subunit and effects on channel function. J Biol Chem 271:26465–26468.

Cohen RM, Foell JD, Balijepalli RC, Shah V, Hell JW, Kamp TJ (2005) Unique modulation of L-type Ca^{2+} channels by short auxiliary β1d subunit present in cardiac muscle. Am J Physiol Heart Circ Physiol 288:H2363–H2374.

Cornet V, Bichet D, Sandoz G, Marty I, Brocard J, Bourinet E, Mori Y, Villaz M, De Waard M (2002) Multiple determinants in voltage-dependent P/Q calcium channels control their retention in the endoplasmic reticulum. Eur J Neurosci 16:883–895.

Dafi O, Berrou L, Dodier Y, Raybaud A, Sauve R, Parent L (2004) Negatively charged residues in the N-terminal of the AID helix confer slow voltage dependent inactivation gating to Ca_V1.2. Biophys J 87:3181–3192.

De Waard M, Scott VE, Pragnell M, Campbell KP (1996) Identification of critical amino acids involved in α1-β interaction in voltage-dependent Ca^{2+} channels. FEBS Lett 380:272–276.

Dolphin AC (2003a) Beta subunits of voltage-gated calcium channels. J Bioenerg Biomembr 35:599–620.

Dolphin AC (2003b) G protein modulation of voltage-gated calcium channels. Pharmacol Rev 55:607–627.

Ertel EA, Campbell KP, Harpold MM, Hofmann F, Mori Y, Perez-Reyes E, Schwartz A, Snutch TP, Tanabe T, Birnbaumer L, Tsien RW, Catterall WA (2000) Nomenclature of voltage-gated calcium channels. Neuron 25:533–535.

Hanlon MR, Berrow NS, Dolphin AC, Wallace BA (1999) Modelling of a voltage-dependent Ca^{2+} channel beta subunit as a basis for understanding its functional properties. FEBS Lett 445:366–370.

Herlitze S, Garcia DE, Mackie K, Hille B, Scheuer T, Catterall WA (1996) Modulation of Ca^{2+} channels by G-protein $\beta\gamma$ subunits. Nature 380:258–262.

Hummer A, Delzeith O, Gomez SR, Moreno RL, Mark MD, Herlitze S (2003) Competitive and synergistic interactions of G protein β2 and Ca^{2+} channel β1b subunits with Ca_V2.1 channels, revealed by mammalian two-hybrid and fluorescence resonance energy transfer measurements. J Biol Chem 278:49386–49400.

Hurley JH, Cahill AL, Currie KP, Fox AP (2000) The role of dynamic palmitoylation in Ca^{2+} channel inactivation. Proc Natl Acad Sci USA 97:9293–9298.

Ikeda SR (1996) Voltage-dependent modulation of N-type calcium channels by G-protein $\beta\gamma$ subunits. Nature 380:255–258.

Jones LP, Wei SK, Yue DT (1998) Mechanism of auxiliary subunit modulation of neuronal alpha1E calcium channels. J Gen Physiol 112:125–143.

Maltez JM, Nunziato DA, Kim J, Pitt GS (2005) Essential $Ca_V\beta$ modulatory properties are AID-independent. Nat Struct Mol Biol 12:372–377.

Meir A, Bell DC, Stephens GJ, Page KM, Dolphin AC (2000) Calcium channel β subunit promotes voltage-dependent modulation of α1B by $G\beta\gamma$. Biophys J 79:731–746.

Neely A, Garcia-Olivares J, Voswinkel S, Horstkott H, Hidalgo P (2004) Folding of active calcium channel β1b-subunit by size-exclusion chromatography and its role on channel function. J Biol Chem 279:21689–21694.

Olcese R, Qin N, Schneider T, Neely A, Wei X, Stefani E, Birnbaumer L (1994) The amino terminus of a calcium channel β subunit sets rates of channel inactivation independently of the subunit's effect on activation. Neuron 13:1433–1438.

Opatowsky Y, Chen CC, Campbell KP, Hirsch JA (2004) Structural analysis of the voltage-dependent calcium channel β subunit functional core and its complex with the α1 interaction domain. Neuron 42:387–399.

Pragnell M, De Waard M, Mori Y, Tanabe T, Snutch TP, Campbell KP (1994) Calcium channel β-subunit binds to a conserved motif in the I-II cytoplasmic linker of the α1-subunit. Nature 368:67–70.

Qin N, Platano D, Olcese R, Costantin JL, Stefani E, Birnbaumer L (1998) Unique regulatory properties of the type 2a Ca^{2+} channel β subunit caused by palmitoylation. Proc Natl Acad Sci USA 95:4690–4695.

Raghib A, Bertaso F, Davies A, Page KM, Meir A, Bogdanov Y, Dolphin AC (2001) Dominant-negative synthesis suppression of voltage-gated cal-

cium channel $Ca_V2.2$ induced by truncated constructs. J Neurosci 21:8495–8504.

Restituito S, Cens T, Barrere C, Geib S, Galas S, De Waard M, Charnet P (2000) The β2a subunit is a molecular groom for the Ca^{2+} channel inactivation gate. J Neurosci 20:9046–9052.

Richards MW, Butcher AJ, Dolphin AC (2004) Ca^{2+} channel β-subunits: structural insights AID our understanding. Trends Pharmacol Sci 25:626–632.

Sandoz G, Lopez-Gonzalez I, Grunwald D, Bichet D, Altafaj X, Weiss N, Ronjat M, Dupuis A, De Waard M (2004) $Ca_V\beta$-subunit displacement is a key step to induce the reluctant state of P/Q calcium channels by direct G protein regulation. Proc Natl Acad Sci USA 101:6267–6272.

Stephens GJ, Page KM, Bogdanov Y, Dolphin AC (2000) The α1B Ca^{2+} channel amino terminus contributes determinants for β subunit-mediated voltage-dependent inactivation properties. J Physiol (Lond) 525:377–390.

Van Petegem F, Clark KA, Chatelain FC, Minor DL Jr (2004) Structure of a complex between a voltage-gated calcium channel β-subunit and an alpha-subunit domain. Nature 429:671–675.

Wakamori M, Mikala G, Mori Y (1999) Auxiliary subunits operate as a molecular switch in determining gating behaviour of the unitary N-type Ca^{2+} channel current in *Xenopus oocytes*. J Physiol (Lond) 517:659–672.

Walker D, Bichet D, Geib S, Mori E, Cornet V, Snutch TP, Mori Y, De Waard M (1999) A new beta subtype-specific interaction in α1A subunit controls P/Q-type Ca^{2+} channel activation. J Biol Chem 274:12383–12390.